RSC Advances

ROYAL SOCIETY OF CHEMISTRY

PAPER

View Article Online
View Journal | View Issue

Cite this: *RSC Adv.*, 2026, **16**, 26909

Synthesis and *in silico* insights of some tetrahydrobenzothienopyrimidine candidates as multi-target antimicrobial, antiproliferative, and antiviral agents

Amna S. Elgubbi,[a] Selwan Hamed,[b] Budur Nuwayji Alanazi,[c] Hoda A. Ahmed[d] and Sayed K. Ramadan *[e]

A new series of fused tri- and tetra-cyclic candidates including a tetrahydrobenzo[*b*]thiophene core was prepared through cyclo-condensation of ethyl formamidate with hydrazine and 2-cyanoethanohydrazide, respectively. The proper locations of amino and imino groups in the first key synthon **2** allowed cyclo-condensation reactions with some carbon electrophiles. The active methylene in the second key synthon **4** condensed with 3-formylpyridine and 2-hydroxybenzaldehyde. Also, thiazolidin-4-one candidate was obtained by condensation of nitrile derivative with mercaptoacetic acid. The purity of compounds obtained was ensured with HPLC analysis. The antimicrobial screening against "two Gram positive strains: *B. subtilis* and *S. aureus*, two Gram negative strains: *E. coli* and *P. aeruginosa* and one fungal strain, *C. albicans*" displayed the promising activity of tetracyclic candidates bearing cyanomethyl, methyl, nitrobenzylidene, or thiazolidinone scaffolds. The cytotoxic effect of promising compounds alone or combined with NAC against liver (HepG2) cancer cell line revealed the highest activity of nitrobenzylidene derivative **8** (IC_{50} = 6.57) followed by thiazolidinone **12** (IC_{50} = 9.76). A strong activity was offered by compounds **4** (IC_{50} = 13.2) and **6** (IC_{50} = 20.34). The antiviral activity against "human adenovirus (HAdV-7) and SARS-CoV-2 (hCoV-19)" indicated the highest potency of cyanomethyl derivative **4** followed by thiazolidinone **12**. To understand the possible mechanisms of antibacterial, antifungal, antitumor, and antiviral actions, molecular docking analyses of potent compounds were investigated toward six target proteins including bacterial (PDB ID: 9JNP and 5TW8), fungal (PDB ID: 4LXJ), tumor (PDB ID: 5NM5), and viral (PDB ID: 5CX6 and 3PY7) proteins compared to their co-crystallized ligands and reference drugs. Most amino acids interacting with the docked compounds were common. Some compounds exhibited the same binding interactions but with different docking scores due to the electronic effects. The highest docking scores were shown by nitrobenzylidene followed by thiazolidinone candidate toward these target proteins except PBP4, which displayed a reverse order. The modeling pharmacokinetics referred to their favorable drug-likeness properties. This work reveals the potential biological profiles of these compounds and provides valuable insights into further therapeutic development.

Received 3rd March 2026
Accepted 8th May 2026

DOI: 10.1039/d6ra01842d

rsc.li/rsc-advances

1. Introduction

Cancer is one of the top causes of death worldwide, accounting for nearly ten million deaths in 2020. Heterocyclic compounds, both natural and synthetic, are well recognized for their pharmacological versatility and serve as structural cores in many clinically approved drugs.[1,2] Recently, the coronavirus (CoV) family has attracted global attention as a major cause of severe respiratory infections. Among them, "Severe Acute Respiratory Syndrome Coronavirus 2 (SARS-CoV-2), the etiological agent of COVID-19", precipitated a global pandemic with profound health and socio-economic consequences. Despite progress in vaccination and public health interventions, the ongoing emergence of viral variants continues to highlight the urgent need for effective antiviral therapies.[3,4] The outbreaks of SARS and COVID-19 have reinforced the importance of developing potent antiviral agents targeting key viral proteins involved in replication and pathogenesis.[5,6]

[a]*Chemistry Department, Faculty of Science, Misurata University, Misurata, 2478, Libya*
[b]*Department of Microbiology and Immunology, Faculty of Pharmacy, Capital University, Ain Helwan, Helwan, 11795, Egypt*
[c]*Department of Chemistry, College of Science, Princess Nourah Bint Abdulrahman University, P.O. Box 84428, Riyadh, 11671, Saudi Arabia*
[d]*Department of Chemistry, College of Science in Yanbu, Taibah University, Yanbu Governorate, Saudi Arabia*
[e]*Chemistry Department, Faculty of Science, Ain Shams University, Cairo, 11566, Egypt. E-mail: sayed.karam2008@sci.asu.edu.eg*

Key components of living cells, such as DNA and RNA, involve heterocyclic frameworks, containing thiophene and pyrimidine cores. Sulfur-containing heterocycles have a wide scale of biological activities due to their structural similarity to numerous naturally occurring and synthetic bioactive molecules.[7–10] Thiophenes, sulfur-containing heterocyclic skeleton, are highly stable aromatic substances with physicochemical characteristics that make them especially valuable in drug design.[11,12] Several thiophene derivatives have been reported to possess significant antitumor and antimicrobial activity.[13–15]

The tetrahydrobenzo[*b*]thiophene scaffold has gained prominence in drug discovery due to its wide scale of biological effects, like antitumor, antimicrobial, antiviral, antioxidant, and analgesic effects.[16–19] Notably, several benzothiophene-based compounds are already in clinical use, highlighting their therapeutic potential across various disease areas. Consequently, the structure–activity relationships (SAR) of these substrates have attracted significant interest from medicinal chemists, aiding in the identification of lead candidates for diverse therapeutic applications. Also, 4,5,6,7-tetrahydrobenzo[*b*]thiophene derivatives have been identified as promising anticancer agents.[20] Some of these compounds exhibit antiproliferative activity by targeting key cancer-related pathways and proteins, including hypoxia-inducible factor-1 alpha (HIF-1α), matrix metalloproteinases 2 & 9 (MMP-2 & MMP-9), vascular endothelial- & epidermal-growth factor receptors (VEGFR & EGFR),[21] human epidermal growth factor receptor 2 (HER2),[22] and colon cancer-associated genes such as collagen type X alpha 1 (COL10A1) and collagen type XI alpha 1 (COL11A1) (see Fig. 1).[23]

Microtubules are dynamic polymers essential for key cellular processes like chromosome segregation, intracellular transport, maintenance of cell structure, and cell division. Given their central role in cell proliferation, modulation of microtule dynamics represents an effective strategy for anticancer drug development. Agents that stabilize or destabilize microtules can induce mitotic arrest and trigger apoptosis, thereby exerting antiproliferative effects. Tubulin, the structural unit of microtules, contains three major drug-binding sites, colchicine, taxane, and vinca alkaloid, targeted by several clinically used chemotherapeutics.[24,25]

In this study, a tetrahydrobenzo[*b*]thiophene scaffold was chosen as the core framework due to its well-documented pharmacological significance. A phenyl ring was kept at position-6 to function as a hydrophobic tail, enhancing structural stability and interactions with hydrophobic pockets of target proteins. To further strengthen the anticancer potential, a pyrimidine ring, recognized for its DNA replication and transcription inhibitory properties,[26] was fused to the core, generating a planar tricyclic system designed for optimal binding with key amino acid residues. Building on our ongoing efforts to develop bioactive heterocyclic scaffolds,[27–33] we focus here on the design and synthesis of a new series of heteroannulated tri- and tetra-cyclic derivatives containing the tetrahydrobenzo[*b*]thiophene core. Their antimicrobial, antiproliferative, and antiviral properties were evaluated, aided by molecular docking and pharmacokinetic modeling approaches.

1.1. Rationale and design

As illustrated in Fig. 1, which shows a series of tetrahydrobenzo[*b*]thiophene-based biological agents, our molecular design strategy was guided by development of two scaffolds featuring the tetrahydrobenzo[*b*]thiophene core linked to a hydrophobic

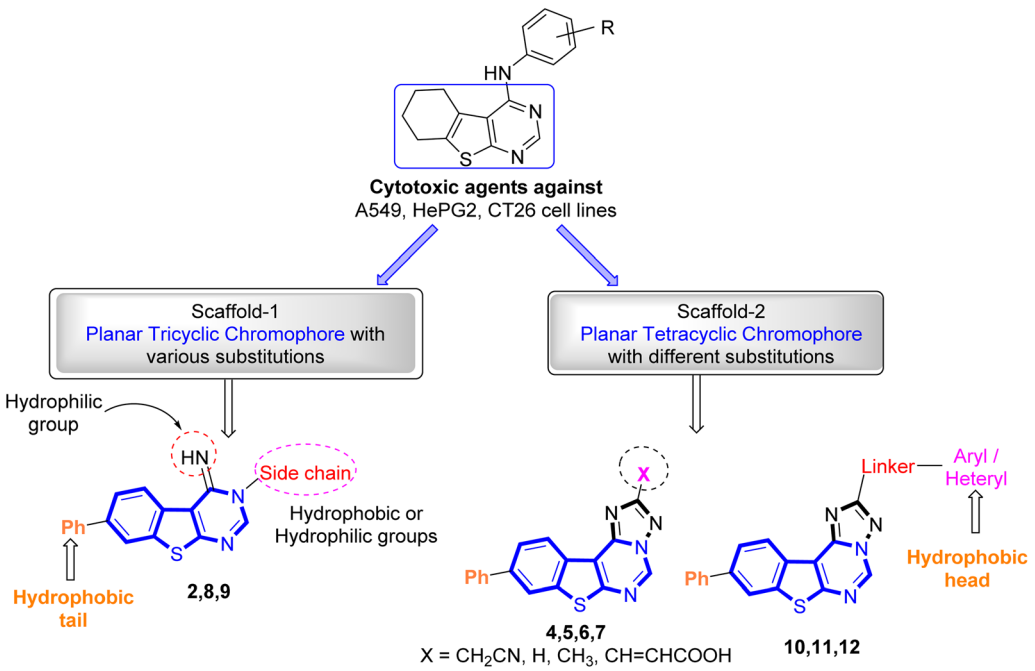

Fig. 1 Models of some reported tetrahydrobenzo[*b*]thiophene biological agents and rationale of molecular design of our target substrates.

tail (phenyl group) at position-6. The first scaffold includes a tricyclic chromophore (tetrahydrobenzo[*b*]theinopyrimidine skeleton like compounds **2**, **8**, and **9**), which bear a hydrophilic (NH) group and incorporate various substituents (hydrophilic and hydrophobic moieties). These substituents were selected to explore how different electronic, hydrophilic, and lipophilic environments affect biological activity of target compounds.

The second frame involved planar tetracyclic chromophores (tetrahydrobenzo[*b*]theinotriazolopyrimidine skeleton) with side chains or linker attached to aryl/hetaryl moieties (as a hydrophobic head) like compounds **4**, **5–7**, and **10–12** as shown in Fig. 1. The two designed platforms aim to incorporate the main pharmacophoric performance; the planar fused tri- and tetra-cyclic skeletons (chromophores) linked with side chains or aryl/hetaryl moieties. Furthermore, the designed targets contain basic N-atoms that were protonated at physiological pH to furnish cationic centers developing their affinity and selectivity.

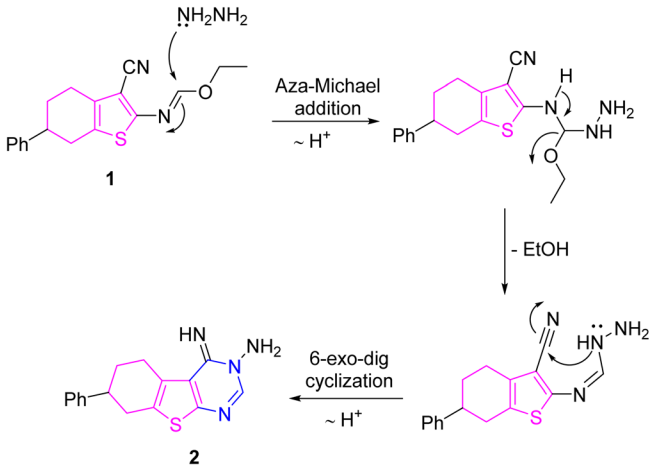

Scheme 2 A possible pathway for the formation of key synthon **2**.

2. Results and discussion

2.1. Chemistry

The key material, ethyl tetrahydrobenzo[*b*]thiophene-2-formamidate **1** was synthesized from 2-aminotetrahydrobenzothiophene-3-nitrile[16] and then reacted with hydrazine hydrate and 2-cyanoethanohydrazide in ethanolic solution to produce two building heteroannulated synthons namely, 4-imino-7-phenyl-5,6,7,8-tetrahydrobenzo[4,5]thieno[2,3-*d*]pyrimidin-3(4*H*)-amine (**2**) and 2-(9-phenyl-8,9,10,11-tetrahydrobenzo[4,5]thieno[3,2-*e*][1,2,4]triazolo-[1,5-*c*]pyrimidin-2-yl)acetonitrile (**4**), respectively (Scheme 1). HPLC analysis showed their elution at a retention time of 7.9 min, and a single sharp peak denoted a purity of 98.8% and 98.9% based on peak area integration, respectively. Absorption bands for NH and NH_2 moieties appeared in IR spectrum of thienopyrimidine **2**, while the nitrile absorption disappeared. Its ^{1}H NMR spectrum displayed two broad singlet signals for NH and NH_2 protons besides a singlet signal for C2–H of pyrimidine ring in the downfield region. The formation of theinopyrimidine **2** could be visualized *via* initial aza-Michael addition of amino group of hydrazine on C=N functionality of substrate **2** to remove ethanol molecule followed by 6-*exo*-dig cyclization (Baldwin's rule) for constructing fused pyrimidine ring (*cf.* Scheme 2).

IR spectrum of tetrahydrobenzothienotriazolopyrimidine **4** retained nitrile absorption. Also, its ^{1}H NMR spectrum disclosed a singlet signal for methylene protons. Compound **4** can be envisioned through initial condensation to remove ethanol molecule and intramolecular 6-*exo*-dig cyclization[34] to construct pyrimidine nucleus as a non-isolable intermediate **3** followed by another intramolecular 5-*exo*-trig ring closure to remove water molecule to get heteroannulated tetracyclic candidate **4** (*cf.* Scheme 3).

The suitable locations of amino and imino groups in candidate **2** allowed them to construct some fused tetracyclic candidates through combination with formic acid, ethanoic anhydride, and maleic anhydride (*cf.* Scheme 4). Indeed, refluxing candidate **2** with formic acid or ethanoic anhydride afforded triazolo-derivatives **5** and **6**, respectively. Using HPLC analysis, they eluted at a retention time of 8.0 min, and a single sharp peak showed a purity of 98.4% and 96.7%, respectively. The absorption bands of NH and NH_2 moieties disappeared in their IR spectra. The ^{1}H NMR spectrum of **6** showed a singlet signal for

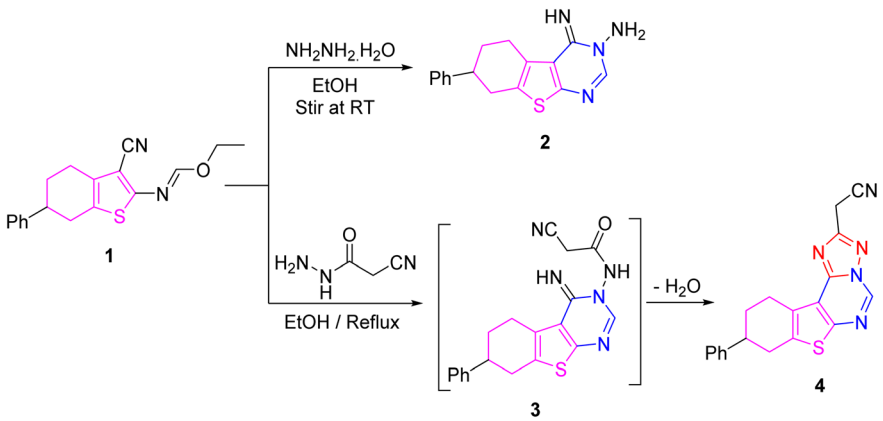

Scheme 1 Reactions of **1** with hydrazine hydrate and 2-cyanoethanohydrazide.

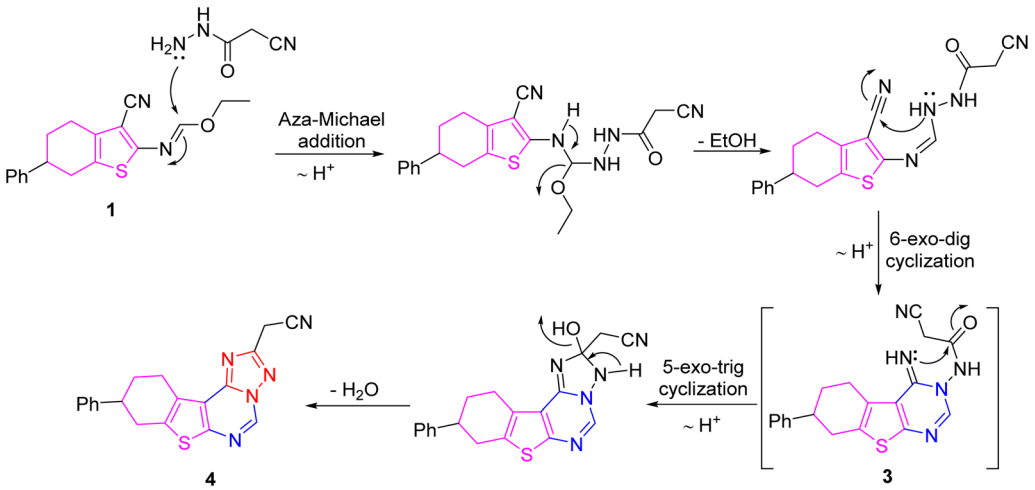

Scheme 3 A plausible pathway for the formation of key synthon **4**.

methyl protons in upfield region. Treatment of candidate **2** with maleic anhydride in refluxing acetic acid afforded acrylic acid derivative **7**, which eluted in HPLC analysis at a retention time of 7.5 min, and a single sharp peak displayed a purity of 99.9%. Absorption bands for hydroxyl and carbonyl groups of carboxylic functionality appeared in its IR spectrum. The *E*-configuration of CH=CH moiety was inferred from its ^{1}H NMR spectrum from which the *J* coupling constants of these doublet signals were 12.4 Hz. Also, a broad singlet signal for carboxylic proton appeared in downfield region (δ 13.58 ppm).

Due to the considerable biological influences of EWG (electron-withdrawing groups),[35] the 4-nitrobenzaldehyde was chosen for condensation with amino compound **2** to produce Schiff base **8**. HPLC analysis depicted its elution at a retention

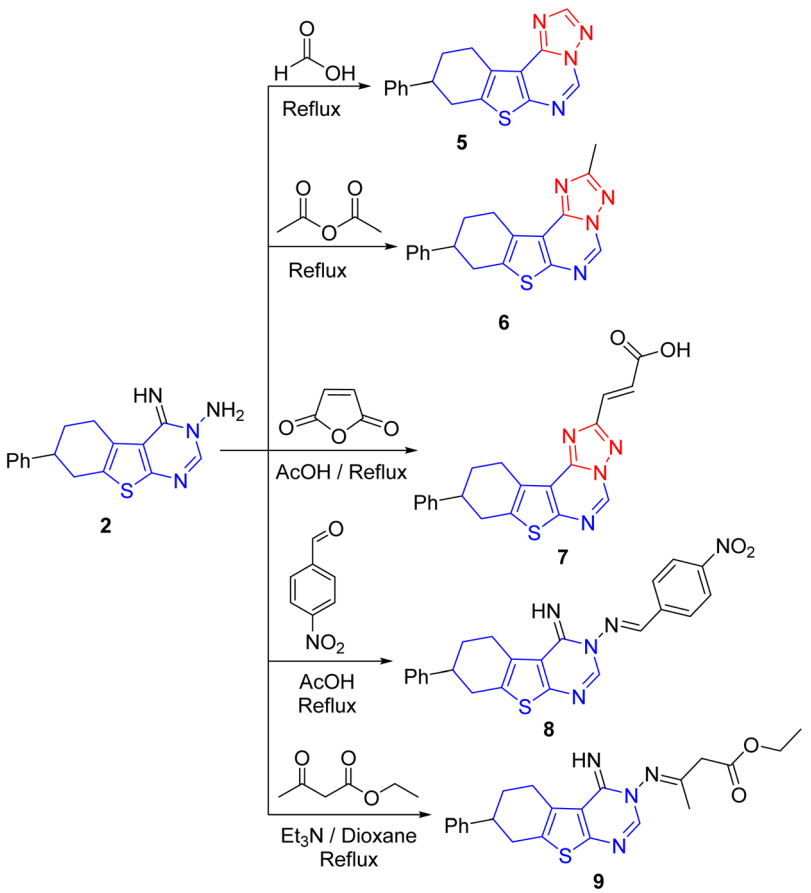

Scheme 4 Synthesis of compounds **5–9**.

time of 8.0 min, and a single sharp peak indicated a purity of 98.7%. The ^{1}H NMR spectrum of Schiff base **8** showed two doublet signals for nitrobenzylidene moiety and a downfield singlet signal for the methine proton (CH═N). Treatment of **2** with ethyl acetoacetate in refluxing 1,4-dioxane including triethylamine afforded the condensation product **9**, which eluted in HPLC analysis at a retention time of 8.0 min, and a sharp single peak denoted a purity of 97.9%. Its ^{1}H NMR spectrum showed triplet and quartet signals for ethyl (–CH_2CH_3) protons, besides singlet signal for CH_2CO and CH_3C═N protons, which confirmed the open structure.

On the other hand, condensation of the nitrile derivative **4** with pyridine-3-carbaldehyde or 2-hydroxybenzaldehyde in refluxing dioxane and piperidine gave α,β-unsaturated nitrile derivatives **10** and **11**, respectively (Scheme 5). HPLC analysis showed their elution at a retention time of 6.78 and 8.0 min, and a sharp single peak indicated a purity of 99.7% and 98.8%, respectively. Their IR spectra showed a lower absorption frequency of nitrile group, confirming its conjugation with the olefinic double bond. In their ^{1}H NMR, a singlet signal of olefinic proton (CH═C) was detected at a higher chemical shift, that was attributed to the electron-withdrawing effect of nitrile group. Finally, thiazolidinone derivative **12** was obtained from treating the nitrile derivative **4** with mercaptoacetic acid in refluxing methanol and pyridine. HPLC analysis implied the elution of thiazolidinone derivative **12** at a retention time of 7.8 min, and a sharp single peak disclosed a purity of 97.7%. In its IR spectrum, the nitrile absorption lacked and new absorption bands for amide C═O and NH groups were detected. Also, its ^{1}H NMR spectrum showed a singlet signal for methylene (CH_2) protons and a broad singlet signal for amide NH proton in downfield region.

A comprehensive nitrosamine risk assessment was conducted, and no significant risk was identified across all steps (*cf.* Materials and methods).

2.2. Antimicrobial activity

The prepared substrates were screened for their antimicrobial effect against five microbial strains, distributed as follows: two Gram positive strains (*Bacillus subtilis* and *Staphylococcus aureus*), two Gram negative strains (*Escherichia coli* and *Pseudomonas aeruginosa*) and one fungal strain (*Candida albicans*). The minimum inhibitory concentrations (MIC, μg mL^{-1}) of the tested compounds were shown in Table 1 using standard broth dilution method.[36] Ofloxacin showed MIC in the range of 2–8 μg mL^{-1} against bacterial strains (*E. coli*, *P. aeruginosa*, *S. aureus*, *B. subtilis*). While ketoconazole had MIC of 1–2 μg mL^{-1} against *C. albicans*. Compared to standard antimicrobial agents, the results revealed the promising effects of compounds **4**, **5**, **6**, **8**, and **12**.

In comparison, our synthesized compounds **4**, **5**, **6**, **8**, and **12** demonstrated MIC values between 50–150 μg mL^{-1} against bacteria and 100–150 μg mL^{-1} against *C. albicans*. Thus, while the prepared compounds are less potent than reference drugs, they still exhibit broad-spectrum inhibitory activity, which is promising given their novel structures and potential for further optimization. To further enhance their activity, we investigated the potential of combining these compounds with antioxidants such as *N*-acetylcysteine (NAC) and vitamin C.

2.2.1. Synergism with antioxidants. Given that oxidative stress and reactive oxygen species (ROS) are leading to microbial pathogenesis and viral replication, antioxidants were explored as potential synergistic partners. By modulating the intracellular redox balance, mitigating ROS-mediated cellular damage, and supporting host immune responses, antioxidants may enhance the biological efficacy of antimicrobial and antiviral agents. On this basis, synergism studies were performed to evaluate whether co-administration of our prepared compounds with antioxidants could amplify their activity. Such

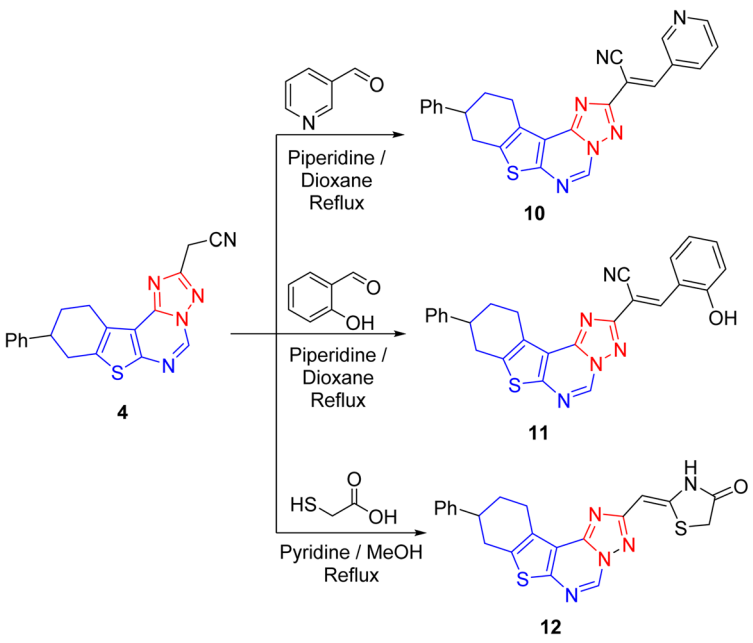

Scheme 5 Synthesis of compounds **10**–**12**.

Table 1 Evaluation of antimicrobial activity and MIC values (μg mL^{-1}) of tested compounds using Ofloxacin (Ofl) and Ketoconazole (Ket) as reference antibacterial and antifungal drugs, respectively[a,b]

	Bacterial strains				Fungi
	Gram negative		Gram positive		
Compds	*E. coli*	*P. aeruginosa*	*S. aureus*	*B. subtilis*	*C. albicans*
1	250 ± 10	250 ± 12	200 ± 10	200 ± 10	500 ± 10
2	250 ± 14	250 ± 10	200 ± 12	200 ± 8	500 ± 15
4[c]	70 ± 4	70 ± 5	60 ± 3	50 ± 4	120 ± 6
5[c]	100 ± 6	100 ± 7	120 ± 8	120 ± 9	150 ± 10
6[c]	100 ± 6	100 ± 7	120 ± 7	120 ± 8	150 ± 10
7	175 ± 8	200 ± 10	150 ± 10	150 ± 9	250 ± 12
8[c]	75 ± 6	80 ± 7	70 ± 5	70 ± 6	100 ± 7
10	175 ± 8	200 ± 10	150 ± 10	150 ± 8	250 ± 12
12[c]	80 ± 5	80 ± 6	100 ± 7	100 ± 8	140 ± 9
Ofl	2 ± 1	4 ± 2	4 ± 2	4 ± 1	—
Ket	—	—	—	—	2 ± 1

[a] All experiments were conducted in triplicate. [b] Positive and negative controls were DMSO and microbial growth, respectively. [c] Are the most promising compounds.

an approach may reduce the required effective dose, thereby improve therapeutic potential while minimize cytotoxic effects.

The synergistic activity of the most promising compounds (**4**, **5**, **6**, **8**, and **12**) in combination with *N*-acetylcysteine (NAC) and vitamin C was assessed (Tables 2 and S1) using checkerboard assay to calculate fractional inhibitory concentration (FIC) index. The results revealed that nitrile derivative **4** showed the strongest synergistic effect, particularly against *B. subtilis* and *C. albicans*. Compounds **5** and **12** also demonstrated marked synergism, especially against *S. aureus* and *B. subtilis*. In comparison, compounds **6** and **8** exhibited moderate but consistent enhancement when combined with antioxidants. Overall, compound **4** emerged as the most effective synergistic candidate, followed by compounds **5** and **12**, indicating their potential for further optimization as combination therapies.

Importantly, these findings suggest that co-formulation with antioxidants may represent a viable therapeutic strategy, enhance the antimicrobial and antifungal efficacy of our synthesized compounds while potentially lower the required dosage and reducing toxicity.

Despite the superior antimicrobial potency of ofloxacin and ketoconazole, the synthesized compounds represent promising candidates in the fight against antimicrobial resistance. Their structural novelty suggests the potential for alternative mechanisms of action, which may help circumvent existing resistance pathways. Moreover, they demonstrated synergistic interactions with *N*-acetylcysteine and vitamin C, evidenced by significant reductions in MIC values, highlighting their potential to enhance therapeutic efficacy, reduce effective dosages, and mitigate the development of drug resistance. While comparison with ofloxacin and ketoconazole provides an appropriate reference framework, the investigated compounds are best considered early-stage leads. At this stage of development, the primary significance of these molecules resides in their structural features and their suitability for subsequent optimization through SAR studies, rather than in achieving potency comparable to clinically established antimicrobial agents. Consequently, these derivatives emerge as valuable lead compounds for development of next-generation antimicrobial agents pointed at combating resistant microbial strains.

2.3. Cytotoxicity testing

The cytotoxic effect of promising compounds (**4**, **5**, **6**, **8**, and **12**) alone or combined with NAC was inspected with different concentrations (25–500 μg mL^{-1}) using MTT (3-[4,5-dimethylthiazole-2-yl]-2,5-diphenyltetrazolium bromide) on HepG2 cancer cell line viability. As noted from the results (Table 3 and Fig. 2), cell viability decreased progressively with

Table 2 Fractional inhibitory concentration indices (FICIs) of *N*-acetylcysteine (NAC) in combination with tested compounds[a,b]

Microorganism	MIC of NAC alone	Compds	MIC alone	MIC with NAC	FICI	Interpretation
S. aureus	1.8	**4**	60	7.5	0.34	Synergistic
		5	120	5	0.26	Synergistic
		6	120	10	0.31	Synergistic
		8	70	10	0.37	Synergistic
		12	100	5	0.27	Synergistic
B. subtilis	1.2	**4**	50	2.5	0.27	Synergistic
		5	120	5	0.38	Synergistic
		6	120	10	0.42	Synergistic
		8	70	10	0.48	Synergistic
		12	100	5	0.38	Synergistic
C. albicans	12.5	**4**	120	5	0.26	Synergistic
		5	150	15	0.13	Synergistic
		6	150	25	0.20	Synergistic
		8	100	25	0.28	Synergistic
		12	140	15	0.14	Synergistic

[a] MIC for tested compounds in μg mL^{-1}, MIC for NAC in mg mL^{-1}. [b] MIC of the most promising compounds were determined in the presence of 0.4 mg per mL NAC.

increasing concentrations of the tested compound, indicating a concentration-dependent cytotoxic effect. Notably, co-treatment with *N*-acetylcysteine (NAC) partially restored cell viability. The IC_{50} (half-maximal inhibitory concentration) were determined. Compound **8** exhibited the highest activity (IC_{50} = 6.57) followed by compound **12** (IC_{50} = 9.76). A strong activity was offered by compounds **4** (IC_{50} = 13.2) and **6** (IC_{50} = 20.34). A moderate activity was displayed by compound **5** (IC_{50} = 23.34). Presumably, EWG (like CN in compound **4** and NO_2 in compound **8**) were reported to show a significant effect of improving the capability to inhibit cancer cell proliferation throughout binding interactions with receptor active sites *via* H-bonding and van-der Waals contacts.

Although cytotoxicity assays provided an initial assessment of the biological effects of the most promising compounds, these findings should be considered preliminary. Comprehensive toxicological studies, including evaluations of mutagenicity, genotoxicity, immunogenicity, and *in vivo* toxicity, are required to fully characterize their safety profiles. Such investigations are planned for future work.

2.4. Inhibition of biofilm production

This experiment aimed to evaluate whether the tested compounds **5**, **6**, and **12** influence biofilm formation of *S. aureus*, *B. subtilis*, and *P. aeruginosa* cultures (10^6 CFU mL^{-1}) and if biofilms provide protection against these compounds using a 96-well plate assay to assess bacterial adherence to an abiotic surface in different times (12, 24, and 48 h).[37] Biofilm formation was then determined by recording the absorbance at 595 nm with a microplate reader (Biotek Elx-808). The reduction in biofilm formation was calculated (Fig. 3) which displayed the promising inhibition of compound **5**.

2.5. Antiviral activity assessment of promising substrates

The antiviral activity of tested compounds (**4**, **5**, **6**, and **12**) was evaluated against human adenovirus (HAdV-7) and SARS-CoV-2 (hCoV-19) applying virus yield reduction and cytopathic effect (CPE) inhibition assays and ribavirin as a standard antiviral agent. The viral titer was calculated using the 50% tissue culture infectious dose ($TCID_{50}$) assay.[38] Different concentrations of tested compounds (40–200 μg mL^{-1}) alone or combined with

Table 3 Percentage of cell viability of HepG2 cancer cell line at different concentrations of tested compounds[a]

Concn. (μg mL^{-1})	4	4 + NAC	5	5 + NAC	6	6 + NAC	8	8 + NAC	12	12 + NAC
500	9.47368	12.23	10.17544	13.5	13.50877	20.54	12.22222	19.5	13.33333	20.23
250	13.50877	16.5	13.68421	23.54	14.5614	26.43	13.4127	23.3	15.55556	29.89
125	41.94444	56.64	14.03509	27.56	21.55556	35.54	21.55556	33.56	27.33333	38.3
100	48.94444	66.45	14.82456	33.6	23.68421	44.61	25.88889	38.9	32.66667	43.5
62.5	53.61111	70.67	65.78947	78.9	55.35088	67.9	27.33333	44.6	40.11111	53.5
50	69.04762	82.23	80.52632	84.5	85.4386	97.5	32.66667	65.3	53.11111	67.9
25	76.66667	92.87	89.29825	105	88.07018	103	48.80952	78.4	66.03175	89.09
IC_{50}%	13.2		23.34		20.34		6.57		9.76	

[a] All experiments were repeated in triplicate, and the presented data were the average results, p value < 0.05.

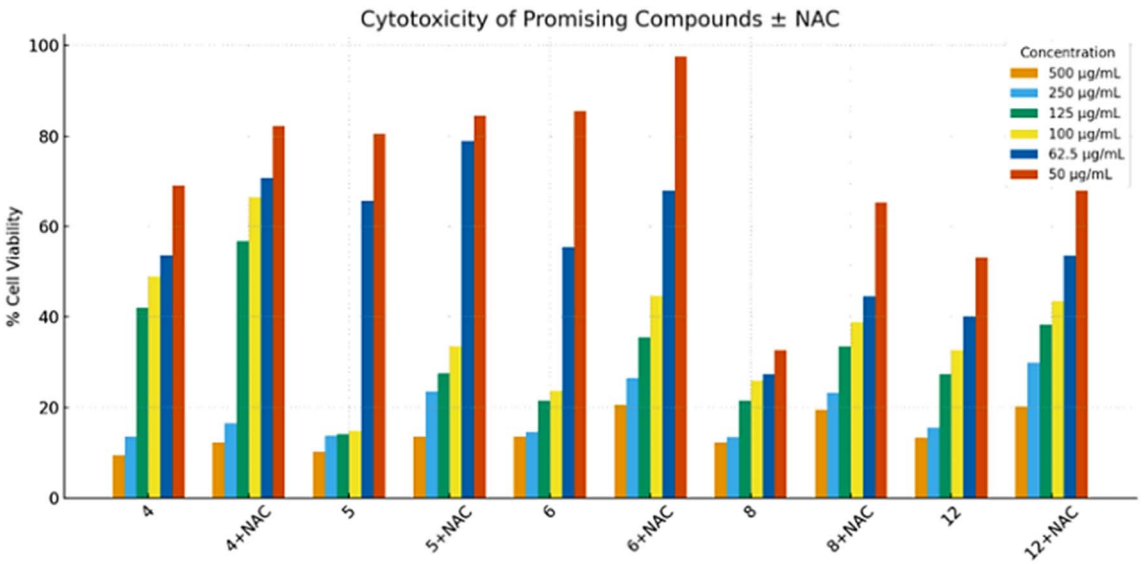

Fig. 2 Cell viability percentage of HepG2 cancer cell line treated with promising compounds (**4**, **5**, **6**, **8**, and **12**) with and without NAC.

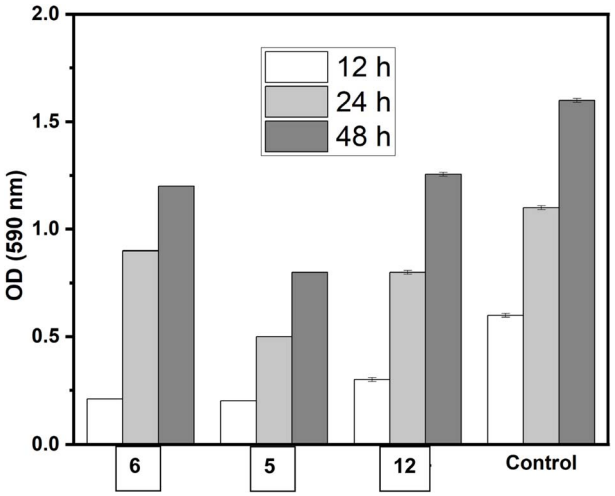

Fig. 3 Percentage inhibition of biofilm formation of the tested compounds **5**, **6**, and **12** compared with control.

0.4 mg mL^{-1} of NAC were used. The number of formed plaques was conducted and compared with negative control (untreated cells) and the percentage reduction was recorded. The results in Table 4 indicated the highest potency of compound **4** (bearing cyanomethyl group) followed by thiazolidinone derivative **12**.

2.6. Structure–activity relationship (SAR)

The antimicrobial activity of the prepared compounds can be correlated with the physicochemical characteristics of their functional groups and the structural differences between Gram-positive and negative bacteria, which represent preliminary trends rather than firm conclusions. The nitrogen-rich heterocyclic scaffold serves as the core pharmacophore, facilitating hydrogen bonding and enhancing target affinity. Electron-withdrawing substituents such as cyano and nitro groups improve binding interactions, while lipophilic moieties, including methyl and phenyl groups, enhance membrane permeability. Hydrazone and amide functionalities provide additional hydrogen-bonding and chelation capabilities, contributing to biological activity. The higher susceptibility of Gram-positive bacteria may be recognized by the absence of an outer membrane, whereas the lipopolysaccharide barrier in Gram-negative bacteria restricts compound penetration.

These findings establish a clear SAR and rationalize the observed antimicrobial profiles of the synthesized derivatives. The experimental potentials of the tested compounds may be visualized with their structures (*cf.* Fig. 4). Initially, the tricyclic system in Schiff base derivative **8** had significant activity owing to the possible H-bond and hydrophobic interactions with nitrobenzylidene moiety. In turn, the essential unit for activity of other compounds was the planar tetracyclic system, tetrahydrobenzo[*b*]theinotriazolopyrimidine skeleton. The inclusion of methyl group (as in compound **6**) changed the lipophilicity and decreased the activity. While the introduction of cyanomethyl group (as electron-withdrawing moiety) increased the activity,[39] as described above. In turn, conducting with a thiazolidinone unit increased the activity through possible H-bond chelation of amide NH–C=O linkage with receptor pockets in addition to pi-interaction of the olefinic moiety.

2.7. Molecular docking

Molecular docking was employed to get preliminary insights into the potential binding modes of the most potent compounds (**4**, **5**, **6**, **8**, and **12**) toward selected bacterial, fungal, tumor, and viral targets, represented by six target proteins. This computational approach was used to predict ligand–protein interactions, binding affinities, and possible modes of molecular recognition. The docking results provide theoretical insights into the stability and orientation of the compounds within active sites; however, these findings remain predictive and do not confirm biological activity. Therefore, further experimental validation through biochemical and molecular assays is required to substantiate the proposed interactions.

For a predictive antibacterial action, a molecular docking simulation was performed against DNA binding protein (ISWI, PDB ID: 9JNP, resolution: 2.3 Å)[40] and wild-type *S. aureus* penicillin-binding protein 4 (PBP4, "PDB ID: 5TW8, resolution: 1.72 Å)".[41] These are considered important bacterial proteins that play a crucial role in antimicrobial drug design through developing research. For predictive antifungal action, it was functioned against lanosterol 14α-demethylase "(PDB ID: 4LXJ, resolution: 1.9 Å)".[42] For a predictive antitumor action, it was performed against tubulin protein (TUB, PDB ID: 5NM5, resolution: 2.05 Å).[43] For a predictive antiviral action, a molecular docking simulation was acted against RNA-dependent RNA polymerase (RdRP, PDB ID: 5CX6, resolution: 2.1 Å)[44] and E6 oncoprotein (PDB ID: 3PY7, resolution: 2.29 Å).[45] These selected targets are partially representative of the tested viruses. RNA-dependent RNA polymerase (RdRP) is a crucial enzyme in SARS-CoV-2 replication, making it a directly relevant target for

Table 4 Percentage reduction in viral replication by selected compounds (**4**, **5**, **6**, and **12**), administered alone or in combination with *N*-acetylcysteine (NAC), against adenovirus and SARS-CoV-2. Values represent the percent inhibition under the tested experimental conditions[a,b]

	4		**5**		**6**		**12**	
% reduction	Alone	**4**/NAC	Alone	**5**/NAC	Alone	**6**/NAC	Alone	**12**/NAC
Adenovirus	90	100	63.70	78	43.70	65	77.5	92
SARS-CoV-2 virus	90	100	70	89	55	75	75	97

[a] Ribavirin was used as a standard antiviral agent that gives 65–72% inhibition. [b] All experiments are performed in triplicates, $p < 0.05$.

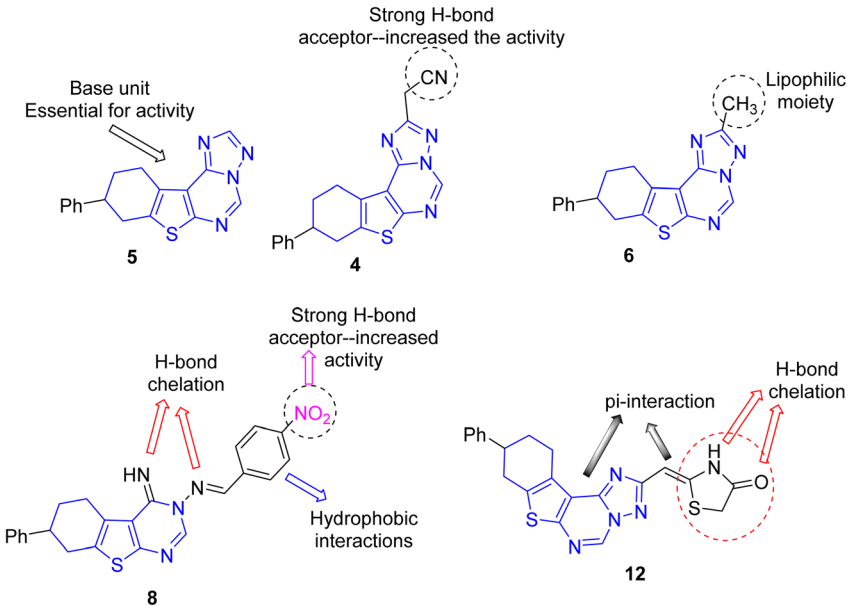

Fig. 4 SAR of the potent compounds, as preliminary trends rather than firm conclusions.

hCoV-19. In contrast, the E6 oncoprotein is not associated with adenovirus (HAdV-7) but originates from human papillomavirus (HPV) and thus does not directly correspond to the adenoviral model used experimentally. Therefore, while RdRP provides a mechanistic link to SARS-CoV-2, the inclusion of E6 reflects a broader antiviral or anticancer targeting strategy rather than a virus-specific match to HAdV-7. These proteins were regained from protein data bank (https://www.rcsb.org).

Co-crystallized ligands were utilized to determine binding sites. Thus, the binding affinities (S, kcal mol^{-1}) of each compound towards the respective target proteins were recorded and compared with their co-crystallized ligands (ATP for ISWI, AI8 for PBP4, LAN for lanosterol 14α-demethylase, CDP for RdRP, GTP for tubulin, CDP for RNA-dependent RNA polymerase, and PRD for E6 oncoproteins) and reference drugs (ofloxacin as reference antibacterial drug, ketoconazole as a reference antifungal drug, and doxorubicin as a reference anticancer drug, paclitaxel as tubulin inhibitor, in addition to cidofovir and remdesivir as antiviral drugs). These antiviral reference drugs were chosen because they are clinically approved and widely recognized as effective against the respective viruses, providing a benchmark to evaluate the relative efficacy of experimental compounds.

The binding poses of each compound were inspected using RMSD (root mean square deviation, Å) to assess their resemblance to the formed crystal structures of protein-ligand complexes (*cf.* Table 5). The binding amino acids with docked substrates and bond types were displayed in Table 6. Most amino acids interacting with the docked compounds were common with those of co-crystallized ligands and references. 2D and 3D interactions of compounds with active pockets of protein targets compared to co-crystallized ligands and reference were shown in Tables S2–S7. Score differences of <0.5 kcal mol^{-1} are supportive evidence for preferable interactions.

Regarding bacterial protein (ISWI), the top docking score was given by substrate **8** (S = −6.943 kcal mol^{-1}, RMSD = 1.566 Å) which was higher than that of co-crystallized ligand ATP (S = −6.452 kcal mol^{-1}, RMSD = 1.499 Å) and reference drug, ofloxacin (S = −5.986 kcal mol^{-1}, RMSD = 1.612 Å). This was achieved by contacts with the key amino acids (common with ATP) including hydrogen bonding of NH to LEU 225, in addition to pi–hydrogen interaction of benzylidene unit with THR 228 and pi–cation interaction of thiophene unit with ARG 266.

Compound **12** exhibited a docking score (−6.249 kcal mol^{-1}, RMSD = 0.832 Å) closer to that of ATP and higher than that of the reference drug. This was through three hydrogen bonding by sulfur, NH, and oxygen with ASN 259, GLN 200, and LEU 196, in addition to two pi–hydrogen contacts by triazolopyrimidine unit with ILE 615. The docking scores of other compounds follow the order: **4** > **5** > **6**, with interactions with common key amino acid residues. With the lowest RMSD value (0.688 Å), compound **5** exhibited pi–cation contact by pyrimidine unit with ARG 266 and two pi–hydrogen interactions by triazolopyrimidine unit with ILE 615.

Regarding bacterial protein 'PBP4', compound **12** had the top S-score (−6.587 kcal mol^{-1}, RMSD = 1.429 Å) followed by compound **8** (S = −6.472 kcal mol^{-1}, RMSD = 1.024 Å), which were closer to that of AI8 (S = −7.759 kcal mol^{-1}, RMSD = 1.775 Å) and higher than that of reference drug, ofloxacin (S = −6.320 kcal mol^{-1}, RMSD = 1.629 Å). Compound **12** exhibited four hydrogen bonding by thiophene–sulfur, thiazolidine–sulfur, methylene, and NH units with SER 139 (common with AI8), GLU 183 (twice), and GLU 114. In turn, compound **8** had hydrogen bonding by nitro-oxygen atom with ARG 186 and pi–hydrogen interaction by phenyl unit with PHE 241 (common with AI8). Compound **4** had two hydrogen bonding by

Table 5 Binding energies (*S*, kcal mol^{-1}) and RMSD values (Å) of the docked substrates toward six target proteins compared to respective co-crystallized ligands and reference drugs

	ISWI		PBP4		Lanosterol 14α-demethylase		Tubulin		RdRP		E6 oncoproteins	
Compds	S^a	RMSD^b	S	RMSD	*S*	RMSD	*S*	RMSD	S	RMSD	*S*	RMSD
4	−5.698	1.248	−6.293	1.318	−6.781	0.904	−5.519	1.016	−5.544	1.344	−6.671	1.732
5	−5.395	0.688	−6.046	0.767	−6.210	1.251	−5.354	1.202	−5.437	1.176	−6.150	1.323
6	−4.656	0.796	−6.182	0.816	−6.462	1.313	−4.799	1.611	−5.458	1.250	−6.366	1.600
8	−6.943	1.566	−6.472	1.024	−8.001	1.616	−6.041	1.478	−6.522	1.350	−6.780	1.825
12	−6.249	0.832	−6.587	1.429	−7.639	1.541	−5.044	1.506	−5.857	1.856	−6.281	0.788
Co-crystallized ligand	−6.452	1.499	−7.759	1.775	−8.219	0.698	−7.029	1.108	−7.850	1.336	−5.087	0.675
Reference drug	−5.986	1.612	−6.320	1.629	−8.859	1.193	−5.333	1.925	−7.236	1.258	−6.365	1.547
Paclitaxel	—	—	—	—	—	—	−6.505	1.821	—	—	—	—

[a] *S*: docking score (kcal mol^{-1}). [b] RMSD in Å.

thiophene–sulfur and nitrile-nitrogen units with GLU 114 and SER 263. It was fortunate that, compound **5** exhibited the lowest RMSD value (0.767 Å).

Concerning fungal protein 'Lanosterol 14α-demethylase', the best docking score was shown by compound **8** (S = −8.001 kcal mol^{-1}, RMSD = 1.616 Å), which was closer to that of LAN (S = −8.219 kcal mol^{-1}, RMSD = 0.698 Å) and ketoconazole (S = −8.859 kcal mol^{-1}, RMSD = 1.193 Å). This was through hydrogen bonding by phenyl-hydrogen with HIS 468 and two pi–hydrogen contacts by benzylidene and phenyl units with TYR 140 and HIS 381. While compound **12** had a docking score of −7.639 kcal mol^{-1} through two hydrogen bonding by thiazolidine– and pyrimidine–nitrogen atoms with MET 509 and TYR 140, in addition to two pi–hydrogen interactions by phenyl and triazole units with VAL 311 and LEU 380. With reasonable RMSD values, the docking scores of other compounds had the following order: **4** > **6** > **5**. Noteworthy, compounds **5** and **6** exhibited the same interactions with bacterial and fungal proteins but they had different docking scores, attributing to the electron-donating effect of methyl group in compound **6**.

According to cancer protein 'tubulin', the superlative docking score was obtained by compound **8** (S = −6.041 kcal mol^{-1}, RMSD = 1.478 Å) which was closer to co-crystallized ligand, GTP (S = −7.029 kcal mol^{-1}, RMSD = 1.108 Å) and paclitaxel (S = −6.505 kcal mol^{-1}, RMSD = 1.821 Å) but higher than that of reference drug, doxorubicin (S = −5.333 kcal mol^{-1}, RMSD = 1.925 Å). It had two pi–hydrogen contacts by pyrimidine and benzylidene units with GLN 11 (common with GTP) and GLU 71. In contrast to bacterial and fungal proteins, the other docking scores toward TUB protein followed the order: **4** > **5** > **12** > **6**. With a lowest RMSD value (1.016 Å), compound **4** offered four hydrogen bonding with the key amino acids, two of them by thiophene–sulfur atom with ASN 101 and GLU 183, and the others by nitrile-nitrogen atom with GLN 15, and ASN 228. In turn, compound **5** exhibited three hydrogen bonding by thiophene–sulfur, pyrimidine–hydrogen, and triazole–nitrogen units with SER 178, VAL 177, and SER 140. Compound **12** showed five hydrogen contacts with the key amino acids SER178, GLN 11, ALA 99, and THR 145 (twice).

Regarding viral protein 'RdRP', compound **8** had the superlative *S*-score (−6.522 kcal mol^{-1}), which was closer to that of CDP (S = −7.850 kcal mol^{-1}) and reference, remdesivir (S = −7.236 kcal mol^{-1}). This was attributed to five hydrogen bonding contacts with the key amino acids GLN 600 (twice), MET 556, ARG 549, and THR 560. Both compounds **12** (S = −5.857 kcal mol^{-1}) and **4** (S = −5.544 kcal mol^{-1}) offered two hydrogen bonding contacts by pyrimidine– and triazole–nitrogen units with GLN 600 and MET 556, and pi–cation interaction by phenyl unit with ARG 549, in addition to three pi–hydrogen interactions by phenyl and triazolopyrimidine units with THR 560, VAL 599 (twice).

Presumably, the relative increase in docking score of compound **12** could be attributed to the extended conjugation of triazole ring with thiazolidine moiety, while it was stopped by the methylene group in compound **4**. The lowest RMSD value (1.176 Å) was shown by compound **5** through proper interactions with the key amino acids, including hydrogen bonding with ARG 549 and pi–cation interaction with ARG 545, in addition to two pi–hydrogen contacts with THR 560 and VAL 599.

With respect to E6 oncoprotein, all compounds exhibited docking scores higher than that of co-crystallized ligand, PRD (S = −5.087 kcal mol^{-1}) and closer to the reference drug, cidofovir (S = −6.365 kcal mol^{-1}). The top docking score was given by substrate **8** (S = −6.780 kcal mol^{-1}) followed by compound **4** (S = −6.671 kcal mol^{-1}). The former showed pi–hydrogen interaction by thiophene unit with TRP 63 and pi–pi contact by phenyl ring with key amino acid, TRY 156 (common with PRD). The latter exhibited two pi–hydrogen interactions by thiophene ring with TRP 63 and PHE 157, in addition to pi–pi contact by triazole ring with TYR 156. Compound **6** showed two hydrogen-pi interactions by pyrimidine and phenyl rings with TRP 341 and TYR 211, in addition to pi–hydrogen contact by phenyl moiety with ASP 15 (common with PRD). Compared with PRD, compound **12** had the lowest RMSD value (0.788 Å) and offered two pi–pi contacts with key amino acid TYR 156 (twice).

Overall, the docking results suggest potential multi-target binding capability of the synthesized compounds, particularly compound **8**, which consistently achieved favorable binding

Table 6 Binding amino acids of docked compounds with six target proteins (ISWI, PBP4, lanosterol 14α-demethylase, tubulin, RdRP, and E6 oncoprotein) compared to their respective co-crystallized ligands and reference drugs

	Binding amino acids (bond type)[a]					
Compds	ISWI	PBP4	Lanosterol 14α-demethylase	Tubulin	RdRP	E6 oncoprotein
4	*GLY 224* (H-acceptor) LEU 225 (H-acceptor) *GLY 226* (H-acceptor) *LYS 227* (H-acceptor) *LYS 227* (H-acceptor) *ARG 614* (pi–cation) *ARG 614* (pi–cation)	GLU 114 (H-donor) SER 263 (H-acceptor)	MET 509 (H-donor) TYR 126 (H-acceptor) TYR 140 (pi–H) LEU 380 (pi–H)	*ASN 101* (H-donor) *GLU 183* (H-donor) *GLN 15* (H-acceptor) *ASN 228* (H-acceptor)	*GLN 600* (H-acceptor) MET 556 (H-acceptor) *ARG 549* (pi–cation) *THR 560* (pi–H) *VAL 599* (pi–H) *VAL 599* (pi–H)	TRP 63 (pi–H) PHE 157 (pi–H) *TYR 156* (pi–pi)
5	*ARG 266* (pi–cation) *ILE 615* (pi–H) *ILE 615* (pi–H)	ARG 300 (H-acceptor) SER 116 (pi–H) *PHE 241* (pi–H)	SER 382 (H-donor) GLY 73 (H-acceptor)	*SER 178* (H-donor) VAL 177 (H-donor) *SER 140* (H-acceptor)	*ARG 549* (H-acceptor) *ARG 545* (pi–cation) *THR 560* (pi–H) *VAL 599* (pi–H)	TRP 341 (H–pi) *TYR 156* (pi–pi) TRP 231 (pi–pi) *TYR 156* (pi–pi)
6	*ARG 266* (pi–cation) *ILE 615* (pi–H) *ILE 615* (pi–H)	ARG 300 (H-acceptor) SER 116 (pi–H) *PHE 241* (pi–H)	SER 382 (H-donor) GLY 73 (H-acceptor)	VAL 177 (H-donor) *ASN 206* (H-acceptor) *ASP 69* (pi–H) *ASN 101* (pi–H) *GLY 144* (pi–H)	*GLN 600* (H-acceptor) MET 556 (H-acceptor) *ARG 549* (pi–cation) *THR 560* (pi–H) *VAL 599* (pi–H) *VAL 599* (pi–H)	TRP 341 (H–pi) TYR 211 (H–pi) *ASP 15* (pi–H)
8	*LEU 225* (H-acceptor) *THR 228* (pi–H) *ARG 266* (pi–cation)	ARG 186 (H-acceptor) *PHE 241* (pi–H)	HIS 468 (H-donor) TYR 140 (pi–H) HIS 381 (pi–H)	*GLN 11* (pi–H) GLU 71 (pi–H)	*GLN 600* (H-acceptor) *GLN 600* (H-acceptor) MET 556 (H-acceptor) *ARG 549* (H-acceptor) *THR 560* (H-acceptor)	TRP 63 (pi–H) *TYR 156* (pi–pi)
12	ASN 259 (H-donor) *GLN 200* (H-donor) LEU 196 (H-acceptor) *ILE 615* (pi–H) *ILE 615* (pi–H)	*SER 139* (H-donor) GLU 183 (H-donor) GLU 183 (H-donor) GLU 114 (H-donor)	MET 509 (H-donor) TYR 140 (H-acceptor) VAL 311 (pi–H) LEU 380 (pi–H)	*SER 178* (H-donor) *GLN 11* (H-acceptor) *ALA 99* (H-acceptor) *THR 145* (H-acceptor) *THR 145* (H-acceptor)	*GLN 600* (H-acceptor) MET 556 (H-acceptor) *ARG 549* (pi–cation) *THR 560* (pi–H) *VAL 599* (pi–H) *VAL 599* (pi–H)	*TYR 156* (pi–pi) *TYR 156* (pi–pi)
Co-crystallized ligands[a]	*ILE 615* (H-donor) *GLN 200* (H-donor) ARG 611 (H-acceptor) *ARG 614* (H-acceptor) *ARG 614* (H-acceptor) *LYS 227* (H-acceptor) ARG 611 (H-acceptor) MET 223 (H-acceptor) *GLY 224* (H-acceptor) *LYS 227* (H-acceptor) *ARG 614* (H-acceptor) *THR 228* (H-acceptor) *THR 228* (H-acceptor) *LEU 225* (H-acceptor) *LYS 227* (H-acceptor)	*SER 139* (H-donor) SER 262 (H-donor) SER 262 (H-donor) GLY 181 (H-donor) SER 75 (H-acceptor) SER 262 (H-acceptor) *SER 139* (H-acceptor) LYS 259 (H-acceptor) THR 260 (H-acceptor) LYS 259 (ionic) LYS 259 (ionic) GLU 297 (ionic) PHE 243 (pi–H) *PHE 241* (pi–pi)	CYS 470 (H-acceptor)	*GLU 183* (H-donor) *ASN 228* (H-donor) *ASN 206* (H-donor) *ASN 101* (H-acceptor) *ASN 101* (H-acceptor) GLY 144 (H-acceptor) *ALA 99* (H-acceptor) *THR 145* (H-acceptor) *THR 145* (H-acceptor) *ASP 69* (H-acceptor) *THR 145* (H-acceptor) GLY 10 (H-acceptor) GLY 143 (H-acceptor) GLY 146 (H-acceptor) *GLN 11* (H-acceptor)	*GLU 601* (H-donor) *ARG 549* (H-acceptor) *THR 560* (H-acceptor) *ARG 545* (H-acceptor) *ARG 545* (H-acceptor) *ARG 549* (H-acceptor) ARG 564 (H-acceptor) *ARG 545* (H-acceptor) *ARG 545* (H-acceptor) ALA 607 (H-acceptor) *GLN 600* (H-acceptor) *GLN 600* (H-acceptor) *ARG 549* (ionic) *ARG 549* (ionic) *ARG 549* (ionic)	*ASP 15* (H-donor) GLU 112 (H-donor) GLU 112 (H-donor) LYS 16 (H-acceptor) *TYR 156* (H–pi)

Table 6 (*Contd.*)

Compds	Binding amino acids (bond type)[a]					
	ISWI	PBP4	Lanosterol 14α-demethylase	Tubulin	RdRP	E6 oncoprotein
	LYS 227 (H-acceptor) GLU 263 (H-acceptor) *GLY 226* (H-acceptor) *ARG 614* (H-acceptor) *ARG 266* (H-acceptor) *GLN 200* (H-acceptor) ARG 611 (ionic) *ARG 614* (ionic) *ARG 614* (ionic) *LYS 227* (ionic) ARG 611 (ionic) ARG 611 (ionic) *LYS 227* (ionic) *ARG 614* (ionic) *ARG 614* (ionic) *LYS 227* (ionic) *TRP 267* (pi–H)			ALA 12 (H-acceptor) *SER 140* (H-acceptor) *ASN 101* (H-acceptor) THR 179 (H-acceptor) *SER 178* (H-acceptor) *GLN 11* (H-acceptor) GLN 15 (H-acceptor) *ASN 228* (H-acceptor) *ASN 206* (H-acceptor)	*ARG 545* (ionic) *ARG 549* (ionic) *ARG 545* (ionic) *ARG 549* (ionic) *ARG 549* (ionic) *ARG 545* (ionic) *ARG 545* (ionic) *VAL 599* (pi–H)	
Reference drugs	ARG 197 (H-acceptor) *ARG 266* (pi–cation) *ARG 266* (pi–cation) *TRP 267* (pi–H)	ASP 264 (H-acceptor) ARG 186 (H-acceptor)	HIS 381 (H-acceptor) PHE 241 (H–pi)	*GLU 183* (H-donor) *GLU 183* (H-donor) *ASN 228* (H-donor) *ASN 206* (H-acceptor) *ASN 228* (H-acceptor)	*GLU 601* (H-donor) *GLU 601* (H-donor) *GLN 600* (H-acceptor) *ARG 549* (H-acceptor) GLY 606 (H-acceptor)	GLU 46 (H-donor) LYS 43 (H-acceptor) GLU 154 (pi–H)
Paclitaxel	—	—	—	*ASN 101* (H-donor) *GLN 11* (H-acceptor)	—	—

[a] The common interacting amino acids between the docked compounds, co-crystallized ligands, and reference drugs were italized.

Table 7 *In silico* evaluation of physicochemical properties of compounds **2–12** compared to paclitaxel and doxorubicin by SwissADME platform

Compds	MW (g mol^{-1})	Clog P^a	TPSA (Å^2)	HBD^b	HBA^c	Lipinski violations	Bioavailability score	GI absorption	log K_p (cm s^{-1})
1	310.41	4.33	73.62	0	3	0	0.55	High	−4.86
2	296.39	2.98	95.93	2	2	0	0.55	High	−6.07
4	345.42	3.51	95.11	0	4	0	0.55	High	−5.74
5	306.38	3.56	71.32	0	3	0	0.55	High	−5.28
6	320.41	3.92	71.32	0	3	0	0.55	High	−5.08
7	376.43	3.48	108.62	1	5	0	0.56	High	−5.71
8	429.49	4.11	128.09	1	5	0	0.55	Low	−5.32
9	408.52	4.29	108.57	1	5	0	0.55	High	−5.81
10	434.52	4.26	108.00	0	5	0	0.55	High	−5.54
11	449.53	4.58	115.34	1	5	0	0.55	Low	−5.12
12	419.52	3.57	125.72	1	4	0	0.55	High	−5.86
Paclitaxel	853.91	3.52	221.29	4	14	2	0.17	Low	−8.91
Doxorubicin	543.52	0.44	206.07	6	12	3	0.17	Low	−8.71

[a] Clog *P*: consensus log *P*. [b] HBD: hydrogen bond donor. [c] HBA: hydrogen bond acceptor.

energies and key residue interactions across multiple proteins. However, these results should be interpreted cautiously as computational predictions that require experimental validation to confirm their biological relevance. While the docking analysis supports the observed antimicrobial activity, it could be interpreted as a predictive tool that proposes plausible mechanisms of action rather than definitive proof of target engagement.

Validation of the docking protocol is performed through calculation of the RMSD, predicted by redocking the co-crystallized ligand on its target enzyme then superimposing the redocked co-crystallized ligand on its native co-crystallized bounded conformation (*cf.* Fig. S1). During this approach, the RMSD values of these proteins were within the proper range.[46,47]

2.8. Modeling pharmacokinetics

The SwissADME tool offers a quick and consistent evaluation of pharmacokinetics and drug-likeness properties, and medicinal chemistry suitability of small substances.[48–50] These molecular features are displayed in Fig. S2–S14 and Table 7. Regarding physicochemical and ADME parameters, these substrates

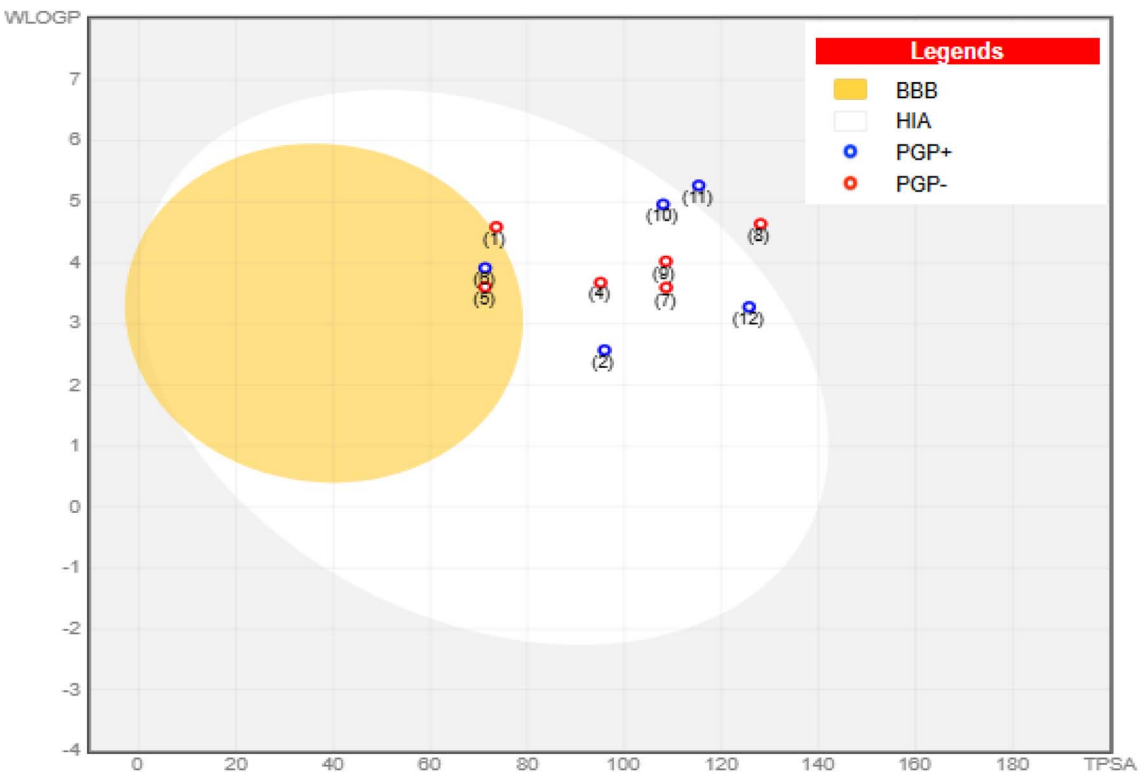

Fig. 5 BOILED-Egg chart of compounds **1–12** compared to paclitaxel and doxorubicin.

satisfy Lipinski, Veber, and Ghose rules, with no violations. Therefore, they can be considered as drug-like candidates. Their molecular weights (MW) follow Lipinski's rule of five (MW < 500 g mol^{-1}). For oral bioavailability, they meet the criteria of potential drug candidates with no more than five hydrogen bond donors (HBD) and ten hydrogen bond acceptors (HBA). In contrast to paclitaxel and doxorubicin, all compounds exhibited good bioavailability scores (0.55 and 0.56). Related to lipophilicity, their calculated MLogP values fall within the suitable scale (<5).

Also, these compounds adhere to the limit of rotatable bond counts as Veber rule. Linked to drug bioavailability, topological polar surface area (TPSA) values for these substrates meet the criterion (<140 $Å^2$) as Veber rule. Except compounds **8** and **11**, other compounds exhibited high gastrointestinal (GI) absorption, resulting in high oral bioavailability (≥0.55). The pink area defined the optimal scale of physicochemical characteristics "(LIPO: lipophilicity 'XLogP3', SIZE: Molecular Weight 'MW', POLAR: polarity 'TPSA', INSOLU: insolubility 'LogS', INSATU: insaturation 'Fraction of Csp^3', FLEX: flexibility 'Rotatable bonds')" for oral administration. Compared to paclitaxel and doxorubicin, these compounds exhibited closer skin permeation ($\log K_p$, cm s^{-1}) values (Table 7).

Regarding the BOILED-Egg plot area (Fig. 5), the compounds **2**, **4**, **7**, **9**, **10**, and **12** were presented in the white area, exhibiting gastrointestinal tract (GIT) absorption. While substrates **5** and **6** were involved in the yellow area, predicting to penetrate the blood–brain barrier (BBB). Indicated by blue color, compounds **2**, **6**, **10**, **11**, and **12** are potential substances for permeability glycoprotein (PGP). Otherwise, compounds **4**, **5**, **7**, **8**, and **9** indicated by red color are not potential substrates for PGP. In consequence, these compounds exhibited appropriate drug-likeness properties.

3. Conclusion

A new series of fused tri- and tetra-cyclic systems incorporating a tetrahydrobenzo[*b*]thiophene core was synthesized starting from an ethyl formamidate synthon. Across the entire synthetic routes, no nitrosating agents were used or generated. While certain steps involved amines, including secondary amines (piperidine) and tertiary amines (triethylamine, pyridine), these were not combined with nitrosating species under conducive conditions (*e.g.*, acidic nitrosation environments). Therefore, the overall risk of nitrosamine formation throughout the synthetic process is considered low. Preliminary antimicrobial screening against two "Gram-positive strains (*B. subtilis* & *S. aureus*), two Gram-negative strains (*E. coli* & *P. aeruginosa*), and one fungal strain (*C. albicans*)" indicated that the tetracyclic candidates, particularly those bearing cyanomethyl, methyl, nitrobenzylidene, or thiazolidinone moieties, exhibited noteworthy activity. Cytotoxicity evaluation against the HepG2 cancer cell line, both for the compounds alone and in combination with NAC, suggested that the nitrobenzylidene derivative displayed the most pronounced effect, followed by the thiazolidinone derivative. Compounds **4** (cyanomethyl) and **6** (methyl) also demonstrated notable cytotoxicity. Assessment of antiviral activity against "human adenovirus type 7 (HAdV-7) and SARS-CoV-2 (hCoV-19)" revealed that the cyanomethyl derivative showed the highest potency, followed by the thiazolidinone compound. Noteworthy, a comprehensive nitrosamine risk assessment will be incorporated in future studies. This will include identifying potential structural alerts, evaluating reagent- and condition-related risks, and investigating possible formation pathways. Additionally, appropriate mitigation strategies will be considered during synthetic route optimization to minimize the likelihood of nitrosamine formation. Such efforts will help improve the safety profile, scalability, and overall robustness of the developed compounds.

To explore potential mechanisms underlying the observed antibacterial, antifungal, antitumor, and antiviral effects, molecular docking analyses were performed for the most active compounds toward six target proteins, including bacterial "(PDB ID: 9JNP and 5TW8)", fungal "(PDB ID: 4LXJ)", tumor "(PDB ID: 5NM5)", and viral "(PDB ID: 5CX6 and 3PY7)" proteins. The docked compounds shared several key interactions with co-crystallized ligands and references. Some variations in docking scores appeared to result from electronic effects. Among the candidates studied, the nitrobenzylidene and thiazolidinone derivatives generally achieved the highest docking scores across most targets, except for PBP4, where the reverse order was observed. Pharmacokinetic modeling suggested favorable drug-like characteristics for these molecules. Collectively, these findings provide preliminary evidence of multi-target biological activity and offer a foundation for further optimization and in-depth biological evaluation.

4. Materials and methods

4.1. Synthesis and characterization

"All solvents and reagents were purified and dried employing standard approaches. The melting points of all substances were taken on a Griffin and George melting-point apparatus. Fourier transform infrared (FT-IR) spectra (ν, cm^{-1}) were determined at PerkinElmer infrared spectrophotometer (version 10.4.2) employing KBr disks. ^{1}H NMR spectra (δ, ppm) were analyzed at 400 MHz on a Bruker Avance III NMR spectrometer employing deuterated dimethyl sulfoxide (DMSO-d_6) solvent with tetramethylsilane (TMS) internal standard. The ^{13}C NMR spectra (δ, ppm) were acquired at 125 MHz on a Bruker Avance III NMR spectrometer. Electron impact mass spectra (EI-MS) were recorded on a Shimadzu GC-MSQP-1000 EX mass spectrometer (Thermo Scientific GCMS MODEL (ISQ LT)) running at 70 eV employing the Thermo X-CALIBUR software at Regional Center for Mycology and Biotechnology (RCMB), Al-Azhar University, Cairo, Egypt. Elemental analyses were recorded on a CHN analyzer at Ain Shams University, and values obtained were within ±0.4 of theoretical values. The homogeneity of the substances obtained was controlled by TLC (thin-layer chromatography) on plates with employing aluminum sheet silica gel 60 F_{254} (Merck, Darmstadt, Germany) with different solvent systems as mobile phases". The purity of compounds was also confirmed by HPLC analysis, and the isolated products were obtained with high chemical purity, while no impurities of

known significant toxicological concern were expected to arise from these synthetic routes.

"The key synthon, ethyl *N*-(3-cyano-6-phenyl-4,5,6,7-tetrahydrobenzo[*b*]thiophen-2-yl)formimidate (**1**) was prepared according to literature".[16]

4.1.1. 4-Imino-7-phenyl-5,6,7,8-tetrahydrobenzo[4,5]thieno[2,3-*d*]pyrimidin-3(4*H*)-amine (2). Hydrazine hydrate (0.25 mL, 5 mmol, 80%) was added dropwise to a stirred solution of ethyl formamidate **1** (1.55 g, 5 mmol) in absolute ethyl alcohol at RT and the reaction mixture was then further stirred for 3 h. The formed solid was then filtered and recrystallized from ethyl alcohol to get beige crystals, mp. 177–179 °C, yield 89%. FT-IR (KBr, ν, cm^{-1}): 3362, 3271, 3166 (NH, NH_2), 1638 (C=N). ^{1}H NMR (400 MHz, DMSO-d_6, δ, ppm): 2.02–2.10 (m, 2H, CH_2), 2.24–2.28 (m, 2H, CH_2), 2.88–2.95 (m, 2H, CH_2), 3.04–3.15 (m, 1H, CH), 4.86 (br.s, 2H, NH_2), 5.98 (br.s, 1H, =NH), 7.27–7.38 (m, 5H, Ar–H), 8.00 (s, 1H, CH=N). ^{13}C NMR (125 MHz, DMSO-d_6, δ, ppm): 27.0, 29.8, 32.8, 40.5, 120.4, 126.7, 127.3 (2), 128.9 (2), 131.24, 131.8, 131.9, 146.1, 148.3, 156.1. EI-MS, 70 eV, *m*/*z* (%): 296.47 ($M^{+\bullet}$, 13), 268.12 (27), 253.05 (16), 241.12 (19), 175.21 (62), 135.10 (25), 114.07 (22), 91.08 (90), 83.12 (39), 79.07 (29). Anal. calcd. for $C_{16}H_{16}N_4S$ (296.39): C, 64.84; H, 5.44; N, 18.90; found: C, 64.76; H, 5.40; N, 18.93%.

4.1.2. 2-(9-Phenyl-8,9,10,11-tetrahydrobenzo[4,5]thieno[3,2-*e*][1,2,4]triazolo[1,5-*c*]pyrimidin-2-yl)acetonitrile (4). A solution of formamidate **1** (1.55 g, 5 mmol) and 2-cyanoethanohydrazide (0.59 g, 5 mmol) in absolute ethyl alcohol (10 mL) was refluxed for 1 h. The solid formed during reflux was filtered and recrystallized from ethyl alcohol to produce beige crystals, mp. 222–223 °C, yield 60%. FT-IR (ν, cm^{-1}): 2214 (C≡N), 1620 (C=N). ^{1}H NMR (400 MHz, DMSO-d_6, δ, ppm): 1.97–2.00 (m, 2H, CH_2), 2.12–2.18 (m, 2H, CH_2), 2.98–3.05 (m, 2H, CH_2), 3.12–3.20 (m, 1H, CHPh), 4.53 (s, 2H, CH_2CN), 7.23–7.37 (m, 5H, Ar–H), 9.63 (s, 1H, C2–H pyrimidine). ^{13}C NMR (125 MHz, DMSO-d_6, δ, ppm): 18.4, 24.9, 29.5, 32.9, 40.8, 116.9, 126.8, 127.3, 128.8 (2), 128.9 (2), 131.3, 137.6, 138.6, 145.8, 145.9, 146.1, 153.9. Anal. calcd. for $C_{19}H_{15}N_5S$ (345.42): C, 66.07; H, 4.38; N, 20.28; found: C, 65.95; H, 4.29; N, 20.31%.

4.1.3. 9-Phenyl-8,9,10,11-tetrahydrobenzo[4,5]thieno[3,2-*e*][1,2,4]triazolo[1,5-*c*]pyrimidine (5). A suspension of **2** (1.11 g, 5 mmol) in formic acid (7 mL) was refluxed for 2 h (TLC). The excess solvent was evaporated then poured portionwise onto cold water with stirring. The solid obtained was filtered, dried, and recrystallized from light petroleum ether/benzene to obtain white crystals, mp. 134–136 °C, yield 75%. FT-IR (KBr, ν, cm^{-1}): 1614 (C=N). ^{1}H NMR (400 MHz, DMSO-d_6, δ, ppm): 2.11–2.16 (m, 2H, CH_2), 2.32–2.35 (m, 2H, CH_2), 3.08–3.12 (m, 2H, CH_2), 3.18–3.27 (m, 1H, CHPh), 7.26–7.39 (m, 5H, Ar–H), 8.44 (s, 1H, CH pyrimidine), 9.22 (s, 1H, CH triazole). ^{13}C NMR (125 MHz, DMSO-d_6, δ, ppm): 25.6, 29.5, 32.9, 40.5, 119.9, 126.9, 127.4 (2), 128.6, 128.9 (2), 137.8, 138.3, 145.7, 148.3, 153.2, 155.2. Anal. calcd. for $C_{17}H_{14}N_4S$ (306.39): C, 66.64; H, 4.61; N, 18.29; found: C, 66.41; H, 4.54; N, 18.27%.

4.1.4. 2-Methyl-9-phenyl-8,9,10,11-tetrahydrobenzo[4,5]thieno[3,2-*e*][1,2,4]triazolo[1,5-*c*]pyrimidine (6). A suspension of **2** (1.11 g, 5 mmol) in acetic anhydride (10 mL) was refluxed for 4 h (TLC). The solid formed while reflux was filtered and recrystallized from ethyl alcohol to furnish white crystals, mp. 186–187 °C, yield 86%. FT-IR (KBr, ν, cm^{-1}): 1615 (C=N). ^{1}H NMR (400 MHz, DMSO-d_6, δ, ppm): 2.12–2.15 (m, 2H, CH_2), 2.31–2.35 (m, 2H, CH_2), 2.69 (s, 3H, CH_3), 3.06–3.10 (m, 2H, CH_2), 3.17–3.26 (m, 1H, CHPh), 7.26–7.39 (m, 5H, Ar–H), 9.09 (s, 1H, C2–H pyrimidine). ^{13}C NMR (125 MHz, DMSO-d_6, δ, ppm): 14.7, 25.7, 29.5, 32.9, 42.1, 126.9, 127.4 (2), 128.6, 128.9 (2), 137.2, 137.3, 137.4, 145.8, 148.9, 149.0, 164.73. Anal. calcd. for $C_{18}H_{16}N_4S$ (320.41): C, 67.47; H, 5.03; N, 17.49; found: C, 67.34; H, 4.96; N, 17.51%.

4.1.5. (*E*)-3-(9-Phenyl-8,9,10,11-tetrahydrobenzo[4,5]thieno[3,2-*e*][1,2,4]triazolo[1,5-*c*]pyrimidin-2-yl)acrylic acid (7). A mixture of **2** (1.11 g, 5 mmol) and maleic anhydride (0.49 g, 5 mmol) in glacial ethanoic acid was refluxed for 2 h (TLC). The solid formed while reflux was collected and recrystallized from ethyl alcohol and 1,4-dioxane (2 : 1) to obtain white crystals, mp. 240–242 °C, yield 79%. FT-IR (KBr, ν, cm^{-1}): 3350 (br. OH), 1704 (C=O), 1614 (C=N). ^{1}H NMR (400 MHz, DMSO-d_6, δ, ppm): 2.01–2.17 (m, 2H, CH_2), 2.95–3.03 (m, 2H, CH_2), 3.15–3.21 (m, 2H, CH_2), 3.37–3.50 (m, 1H, CHPh), 6.51 (d, 1H, CH^{β}=CH^{α}, J = 12.4 Hz), 6.95 (d, 1H, CH^{β}=CH^{α}, J = 12.4 Hz), 7.24–7.35 (m, 5H, Ar–H), 9.58 (s, 1H, C2–H pyrimidine), 13.58 (br.s, 1H, COOH). ^{13}C NMR (125 MHz, DMSO-d_6, δ, ppm): 25.3, 29.4, 32.8, 40.5, 119.4, 124.3, 126.9, 127.4 (2), 128.6 (2), 128.9, 130.7, 137.6, 138.8, 145.7, 148.3, 153.7, 161.0, 167.5. Anal. calcd. for $C_{20}H_{16}N_4O_2S$ (376.43): C, 63.81; H, 4.28; N, 14.88; found: C, 63.70; H, 4.22; N, 14.86%.

4.1.6. 3-((4-Nitrobenzylidene)amino)-7-phenyl-5,6,7,8-tetrahydrobenzo[4,5]thieno[2,3-*d*]pyrimidin-4(3*H*)-imine (8). A solution of **2** (1.11 g, 5 mmol) and 4-nitrobenzaldehyde (0.75 g, 5 mmol) in glacial acetic acid (10 mL) was refluxed for 30 min (TLC). The solid formed was filtered and recrystallized from ethyl alcohol to give red crystals, mp. 235–237 °C, yield 81%. FT-IR (KBr, ν, cm^{-1}): 3337 (NH), 1622 (C=N), 1521, 1338 (NO_2). ^{1}H NMR (400 MHz, DMSO-d_6, δ, ppm): 2.12–2.23 (m, 2H, CH_2), 2.37–2.40 (m, 2H, CH_2), 2.93–3.01 (m, 2H, CH_2), 3.08–3.15 (m, 1H, CHPh), 5.62 (br.s, 1H, =NH), 7.28–7.82 (m, 5H, Ar–H), 8.38 (d, 2H, 2 CH^m nitrophenyl, J = 8.4 Hz), 8.42 (s, 1H, C2–H pyrimidine), 8.55 (d, 2H, 2 CH^o nitrophenyl, J = 8.4 Hz), 9.23 (s, 1H, CH=N). ^{13}C NMR (125 MHz, DMSO-d_6, δ, ppm): 24.2, 29.8, 33.9, 40.5, 124.2, 124.4, 124.5, 127.3 (2), 127.4, 128.8 (2), 128.9 (2), 130.8 (2), 130.9, 133.4, 137.5, 139.0, 147.9, 150.9, 153.5. Anal. calcd. for $C_{23}H_{19}N_5O_2S$ (429.50): C, 64.32; H, 4.46; N, 16.31; Found: C, 64.20; H, 4.39; N, 16.28%.

4.1.7. Ethyl 3-((4-imino-7-phenyl-5,6,7,8-tetrahydrobenzo[4,5]thieno[2,3-*d*]pyrimidin-3(4*H*)-yl)imino)butanoate (9). A mixture of **2** (1.11 g, 5 mmol) and ethyl acetoacetate (0.65 g, 5 mmol) in dry 1,4-dioxane containing Et_3N (0.1 mL) was refluxed for 1 h. The solid formed upon reflux was filtered and recrystallized from ethanol to get white crystals, mp. 220–222 °C, yield 53%. FT-IR (KBr, ν, cm^{-1}): 3108 (NH), 1735 (C=O ester), 1638 (C=N). ^{1}H NMR (400 MHz, DMSO-d_6, δ, ppm): 1.51 (t, 3H, CH_2CH_3, J = 7.2 Hz), 1.93–1.99 (m, 2H, CH_2), 2.15 (s, 3H, CH_3), 2.78–2.86 (m, 2H, CH_2), 2.97 (s, 2H, CH_2CO), 3.03–3.17 (m, 2H, CH_2), 3.34–3.57 (m, 1H, CHPh), 4.10 (q, 2H, OCH_2, J = 7.2 Hz), 6.49 (br.s, 1H, =NH), 7.24–7.36 (m, 5H, Ar–H), 9.52 (s, 1H, C2–H pyrimidine). ^{13}C NMR (125 MHz, DMSO-d_6, δ, ppm): 14.4, 26.5,

29.5, 40.4, 60.1, 66.8, 127.3, 127.4 (2), 128.8 (2), 128.9, 132.1, 133.2, 134.3, 137.6, 139.2, 142.5, 145.6, 146.2, 159.5, 162.4. Anal. calcd. for $C_{22}H_{24}N_4O_2S$ (408.52): C, 64.68; H, 5.92; N, 13.71; Found: C, 64.52; H, 5.85; N, 13.68%.

4.1.8. 2-(9-Phenyl-8,9,10,11-tetrahydrobenzo[4,5]thieno [3,2-*e*][1,2,4]triazolo[1,5-*c*]pyrimidin-2-yl)-3-(pyridin-3-yl) acrylonitrile (10). A solution of nitrile derivative **4** (1.81 g, 5 mmol) and 3-formylpyridine (0.535 g, 5 mmol) in 1,4-dioxane (10 mL) containing piperidine (0.3 mL) was refluxed for 2 h. The solid formed was filtered while hot and recrystallized from ethyl alcohol/dioxane to get beige crystals, mp. 261–262 °C, yield 45%. FT-IR (KBr, ν, cm^{-1}): 2229 (C≡N), 1611 (C=N). ^{1}H NMR (400 MHz, DMSO-d_6, δ, ppm): 2.05–2.16 (m, 2H, CH_2), 2.99–3.10 (m, 2H, CH_2), 3.12–3.15 (m, 2H, CH_2), 3.21–3.37 (m, 1H, CHPh), 7.28–7.60 (m, 6H, Ar–H), 8.40–8.45 (m, 2H, Ar–H pyridine), 8.71 (s, 1H, CH=), 9.08 (s, 1H, C2–H pyridine), 9.65 (s, 1H, C2–H pyrimidine). Anal. calcd. for $C_{25}H_{18}N_6S$ (434.52): C, 69.10; H, 4.18; N, 19.34; found: C, 69.01; H, 4.13; N, 19.35%.

4.1.9. 3-(2-Hydroxyphenyl)-2-(9-phenyl-8,9,10,11-tetrahydrobenzo[4,5]thieno[3,2-*e*][1,2,4]triazolo[1,5-*c*]pyrimidin-2-yl)acrylonitrile (11). A mixture of nitrile derivative **4** (1.81 g, 5 mmol) and 2-hydroxybenzaldehyde (0.61 g, 5 mmol) in 1,4-dioxane (10 mL) containing piperidine (0.5 mL) was refluxed for 2 h. The solid formed during reflux was filtered and then recrystallized from dioxane to get yellow crystals, mp. 298–299 °C, yield 89%. FT-IR (KBr, ν, cm^{-1}): 3297 (br. OH), 2203 (C≡N), 1644 (C=N). ^{1}H NMR (400 MHz, DMSO-d_6, δ, ppm): 2.04–2.17 (m, 2H, CH_2), 2.87–3.00 (m, 2H, CH_2), 3.12–3.15 (m, 2H, CH_2), 3.37–3.57 (m, 1H, CHPh), 6.97 (d, 1H, Ar–H, $J = 7.9$ Hz), 7.02 (d, 2H, Ar–H, $J = 8.2$ Hz), 7.24–8.18 (m, 5H, Ar–H), 8.23 (d, 1H, Ar–H, $J = 8.3$ Hz), 8.79 (s, 1H, CH=), 9.62 (s, 1H, C2–H pyrimidine), 10.45 (br.s, 1H, OH). Anal. calcd. for $C_{26}H_{19}N_5OS$ (449.53): C, 69.47; H, 4.26; N, 15.58; found: C, 69.32; H, 4.19; N, 15.61%.

4.1.10. 2-((9-Phenyl-8,9,10,11-tetrahydrobenzo[4,5]thieno [3,2-*e*][1,2,4]triazolo[1,5-*c*]pyrimidin-2-yl)methylene) thiazolidin-4-one (12). A mixture of nitrile derivative **4** (1.81 g, 5 mmol) and thioglycolic acid (0.46 g, 5 mmol) in methyl alcohol (20 mL) including pyridine (0.5 mL) was refluxed for 6 h then poured portionwise onto crushed ice and acidified with diluted hydrochloric acid (3 mL, 10%) with stirring. The formed solid was filtered, dried, and crystallized from ethyl alcohol/dioxane to obtain beige crystals, mp. 227–229 °C, yield 69%. FT-IR (KBr, ν, cm^{-1}): 3200 (NH), 1708 (C=O), 1615 (C=N). ^{1}H NMR (400 MHz, DMSO-d_6, δ, ppm): 2.03–2.15 (m, 2H, CH_2), 3.01–3.04 (m, 2H, CH_2), 3.12–3.19 (m, 2H, CH_2), 3.24–3.37 (m, 1H, CHPh), 4.52 (s, 2H, CH_2), 6.12 (s, 1H, CH=), 7.23–7.36 (m, 5H, Ar–H), 9.62 (s, 1H, C2–H pyrimidine), 11.39 (br.s, 1H, NH). ^{13}C NMR (125 MHz, DMSO-d_6, δ, ppm): 18.3, 25.6, 29.4, 32.9, 40.5, 117.1, 119.5, 126.9, 127.4 (2), 128.5 (2), 128.9, 137.5, 137.6, 138.6, 145.7, 149.3, 153.8, 153.9, 159.4. Anal. calcd. for $C_{21}H_{17}N_5OS_2$ (419.52): C, 60.12; H, 4.08; N, 16.69; found: C, 60.02; H, 4.01; N, 16.67%.

4.2. Nitrosamine risk assessment of the synthetic routes

All experiments were performed under restricted precautions in fuming hood. Also, the pH and reaction conditions were controlled to prevent nitrosamine formation, which was confirmed by HPLC analysis. The nitrosating conditions were avoided from ever coexisting with amines, and there were no nitrosating agents/nitrite sources at the synthetic stages and workup of products. A comprehensive nitrosamine risk assessment was conducted for all steps in the synthetic pathway based on the presence of amine-containing reagents, potential nitrosating agents, and reaction conditions, in line with current expectations from FDA and EMA.

• Synthesis of compound **2**: hydrazine hydrate was added dropwise to a stirred solution of ethyl formamidate **1** in absolute ethanol at ambient temperature, and the reaction mixture was stirred for 3 h. This step involves hydrazine hydrate, a nitrogen-containing reagent; however, no secondary or tertiary amines are present. No nitrosating agents (*e.g.*, nitrite salts, nitric acid, or nitrogen oxides) were used or expected to form. The reaction was conducted in ethanol under neutral conditions at room temperature, which are not conducive to nitrosamine formation.

Risk assessment: low risk.

• Synthesis of compound **4**: ethyl formamidate **1** reacted with 2-cyanoethanohydrazide in ethanol under reflux. Although nitrogen-containing species were present, no secondary amines or nitrosating agents were involved. The reaction medium (ethanol) and absence of acidic nitrosating conditions reduce the likelihood of nitrosamine formation.

Risk assessment: low risk.

• Synthesis of compound **5**: compound **2** was refluxed in formic acid. Formic acid provided acidic conditions; however, no nitrite or nitrosating agents were present. In the absence of nitrosating species, acidic conditions alone do not lead to nitrosamine formation.

Risk assessment: low risk.

• Synthesis of compound **6**: compound **2** was refluxed in acetic anhydride. No nitrosating agents or nitrite sources were present. Although acetylation occurred under heated conditions, there is no combination of amines with nitrosating species.

Risk assessment: low risk.

• Synthesis of compound **7**: compound **2** reacted with maleic anhydride in glacial acetic acid under reflux. Glacial acetic acid provides acidic conditions; however, no nitrite or nitrosating agents were present. Therefore, nitrosamine formation is not expected.

Risk assessment: low risk.

• Synthesis of compound **8**: compound **2** reacted with 4-nitrobenzaldehyde in glacial acetic acid under reflux. Despite the presence of a nitro group, it does not act as a nitrosating agent under these conditions. No nitrite species are present.

Risk assessment: low risk.

• Synthesis of compound **9**: compound **2** reacted with ethyl acetoacetate in dry 1,4-dioxane in the presence of triethylamine. Triethylamine is a tertiary amine; however, no nitrosating agents were present in this step. In the absence of nitrite species, the formation of nitrosamines is not expected.

Risk assessment: low risk.

• Synthesis of compound **10**: nitrile derivative **4** reacted with 3-formylpyridine in 1,4-dioxane in the presence of piperidine. Piperidine is a secondary amine and represents a potential nitrosamine precursor. However, no nitrosating agents were used or expected. The reaction was carried out under non-nitrosating conditions.

Risk assessment: low risk (with awareness due to secondary amine presence).

• Synthesis of compound **11**: nitrile derivative **4** reacted with 2-hydroxybenzaldehyde in 1,4-dioxane in the presence of piperidine. Similar to the previous route, piperidine is present; however, no nitrosating agents were involved.

Risk assessment: low risk (with awareness due to secondary amine presence).

• Synthesis of compound **12**: nitrile derivative **4** reacted with thioglycolic acid in methanol in the presence of pyridine, followed by acidification with dilute hydrochloric acid. Although acidic conditions are introduced during workup and pyridine (a tertiary amine) is present, no nitrosating agents were used. Therefore, nitrosamine formation is not expected.

Risk assessment: low risk.

Thus, across the entire synthetic route, no nitrosating agents (*e.g.*, nitrites or nitrogen oxides) are used or generated. While certain steps involve amines, including secondary amines (piperidine) and tertiary amines (triethylamine, pyridine), these are not combined with nitrosating species under conducive conditions (*e.g.*, acidic nitrosation environments). Therefore, the overall risk of nitrosamine formation throughout the synthetic process is considered low. Nevertheless, standard controls such as the use of high-purity reagents and solvents and minimization of potential nitrite impurities are recommended to further mitigate any theoretical risk.

4.3. Antimicrobial activity

Five microbial strains were also used; "*E. coli* O157:H7 ATCC 51659 and *C. albicans* ATCC 90028 were purchased from Egyptian Microbial Culture Collection (EMCC)", Faculty of Agriculture, Ain Shams University. While *B. subtilis* ATCC6051, *S. aureus* ATCC 9144 and *P. aeruginosa* ATCC 27853 were a gift from "Department of Microbiology and Immunology, Faculty of Pharmacy, Tanta University". Positive and negative controls were microbial growth and DMSO, respectively.[51,52] Ketoconazole (Ket) was used as reference antifungal drug. Ofloxacin (Ofl) was used as reference antibacterial drug.

"Muller Hinton (MH), Sabouraud dextrose agar, and broth were generally used for bacterial and fungal growth respectively, at 37 °C for 24–30 h. *Vero* and HepG2 cell lines were grown on Dulbecco's Modified Eagle medium (DMEM) that was supplemented with 10% fetal bovine serum and 0.1% antibiotic/antimycotic solution. All growth media and reagents used in this study were purchased form Sigma/Aldrich, USA, Oxoid, UK, and Fluka, Switzerland".

4.3.1. Determination of MIC. "The MIC of the tested chemicals were determined using the standard broth dilution method according to CLSI guidelines.[36] In brief, overnight cultures of standard microbial isolates were diluted 1 : 1000 to obtain a final concentration of 1–2 $\times$ 10^5 CFU mL^{-1}. MIC values were measured using a two-fold serial dilution across a concentration range of 7.8 to 1000 μg mL^{-1}. The cultures were then incubated at 37 °C with continuous shaking at 150 rpm, and the results were assessed by measuring optical density at 600 nm. All experiments were conducted in triplicate. Stock solution of the tested compounds was 5 mg mL^{-1}, starting with a concentration of 1 mg mL^{-1} (1000 μg mL^{-1})".

4.3.2. Synergism with antioxidants. "The synergistic effect of the selected compounds in combination with *N*-acetylcysteine (NAC) and vitamin C was assessed using the checkerboard method to determine the fractional inhibitory concentration (FIC) index. In this approach, a 96-well plate was used, where antimicrobial agents were serially diluted along the *x*-axis, while NAC was diluted along the *y*-axis, each in equal volumes. The plates were then incubated at 37 °C for 24 h".[53] Experiments were repeated in triplicate.

4.3.3. Cytotoxic activity. The cytotoxic effect of promising compounds alone or combined with NAC (**4**, **5**, **6**, **8**, and **12**) was evaluated with different concentrations (25–500 μg mL^{-1}) using MTT on HepG2 cell viability. The experiment was carried out at VACSERA Co., Egypt. In summary, 0.5 $\times$ 10^5 cells per well in serum-free medium were plated in flat bottom 96-well microplate and exposed to 20 μL of various doses 1–500 μg mL^{-1} of the investigated compounds alone or combined with NAC, at concentration of 1.5 mg mL^{-1} over 48 h at 37 °C in 5% CO_2. Following 4 h of incubation, the media were withdrawn, 40 μL of MTT solution/well was applied, and the absorbance at 570 nm was measured photometrically using an ELISA reader for microplates.[53] The experiment was conducted in triplicate.

4.3.4. Inhibition of biofilm production. A 96-well plate assay was employed to assess bacterial adherence to an abiotic surface.[37] In this method, *S. aureus*, *B. subtilis*, and *P. aeruginosa* cultures (10^6 CFU mL^{-1}) were incubated in vinyl U-bottom 96-well microtiter plates with subinhibitory concentrations (40–80 μg mL^{-1}) of the selected compounds. After 24 h of incubation at 37 °C, non-adherent (planktonic) bacteria were removed by rinsing, while the remaining biofilm-forming bacteria were stained using crystal violet dye. "Biofilm formation was then quantified by measuring absorbance at 595 nm with a microplate reader (Biotek Elx-808), where the intensity of the stain reflected bacterial attachment and biofilm development. The reduction in biofilm formation was calculated using the following formula":[54]

$$\text{Percentage inhibition} = 100 - \left[\frac{A_{590}\ \text{nm experimental well}}{A_{590}\ \text{nm control well without treatment}} \times 100\right]$$

4.3.5. Assessment of antiviral activity. "The antiviral activity of the test compounds was evaluated using a virus yield reduction assay and cytopathic effect (CPE) inhibition assay. *Vero* cells were cultured in DMEM supplemented with 10% fetal bovine serum (FBS), 1% penicillin–streptomycin (100 U mL^{-1}), and 2 mM L-glutamine. The cells were maintained at 37 °C in a humidified incubator with 5% CO_2 and were sub-cultured

every 2–3 days upon reaching 80–90% confluence. Then, human adenovirus (HAdV-7) and SARS-CoV-2 (hCoV-19) were propagated in 1.5–2 $\times$ 10^4 *Vero* cells per well by infecting monolayers at an appropriate multiplicity of infection (MOI) and incubating until CPE were observed. The viral titer was determined using the 50% Tissue Culture Infectious Dose ($TCID_{50}$) assay following standard protocols.[55] Vero cells were treated with the test compound for 2–3 h before viral infection, then washed and infected with the virus. Then culture medium containing different concentrations of tested compounds (40–200 μg mL^{-1}) alone or combined with 0.4 mg mL^{-1} of NAC were added and incubated for a further 72 h. The number of formed plaques was determined and compared with negative control (untreated cells), and the percentage reduction was determined".

Conflicts of interest

No potential conflict of interest was reported by the authors.

Data availability

All data generated or analyzed during this study are included in this article and its supplementary information (SI). Supplementary information: spectral data. See DOI: https://doi.org/10.1039/d6ra01842d.

Acknowledgements

Princess Nourah Bint Abdulrahman University Researchers Supporting Project number (PNURSP2026R923), Princess Nourah Bint Abdulrahman University, Riyadh, Saudi Arabia.

References

1 E. Mansour, A. A. Abd-Rabou, S. S. Zaghlool, A. M. Sayed, I. F. Nassar and S. I. Elewa, *J. Mol. Struct.*, 2025, **1331**, 141471.
2 J. Y. Al-Humaidi, S. M. Gomha, L. A. Albedair, *et al.*, *Curr. Org. Synth.*, 2025, **22**(3), 371–382.
3 C. Liu, *et al.*, Research and Development on Therapeutic Agents and Vaccines for COVID-19 and Related Human Coronavirus Diseases, *ACS Cent. Sci.*, 2020, **6**(3), 315–331.
4 A. Dutta, A. Roy, L. Roy, S. Chattopadhyay and S. Chatterjee, Immune response and possible therapeutics in COVID-19, *RSC Adv.*, 2021, **11**, 960–977.
5 Z. B. Milanovic, *et al.*, Inhibitory activity of quercetin, its metabolite, and standard antiviral drugs towards enzymes essential for SARS-CoV-2: the role of acid–base equilibria, *RSC Adv.*, 2021, **11**, 2838–2847.
6 A. R. Morsy, S. H. Mahmoud, N. M. Abou Shama, W. Arafa, G. A. Yousef, A. A. Khalil and S. K. Ramadan, Antiviral activity of pyrazole derivatives bearing a hydroxyquinoline scaffold against SARS-CoV-2, HCoV-229E, MERS-CoV, and IBV propagation, *RSC Adv.*, 2024, **14**, 27935.
7 H. R. Elgiushy, N. A. Abou-Taleb, G. G. Holz, *et al.*, *Bioorg. Chem.*, 2021, **114**, 105079.
8 F. O. Ashmawy, S. M. Gomha, M. A. Abdallah, *et al.*, *Molecules*, 2023, **28**(11), 4270.
9 A. I. Khodair, A. I. Metwally, N. A. Kheder and M. M. T. El-Tahawy, *J. Mol. Struct.*, 2024, **1303**, 137565.
10 S. I. Elewa, E. Mansour, I. F. Nassar and A. A. I. Mekawey, *Russ. J. Bioorg. Chem.*, 2020, **46**, 382–392.
11 A. S. Elgubbi, E. A. E. El-Helw, A. Y. Alzahrani and S. K. Ramadan, *RSC Adv.*, 2024, **14**(9), 5926–5940.
12 I. F. Nassar and N. S. M. Ismail, *Organic & Medicinal Chemistry International Journal*, 2023, **12**(5), 555847.
13 S. M. Gomha, S. M. Riyadh, B. Huwaimel, M. E. M. Zayed and M. H. Abdellattif, *Molecules*, 2022, **27**(14), 4639.
14 S. R. Abd El Hadi, D. S. Lasheen, M. A. Hassan and K. A. M. Abouzid, *Arch. Pharm.*, 2016, **349**(11), 827–847.
15 A. Archna, S. Pathania and P. A. Chawla, *Bioorg. Chem.*, 2020, **101**, 104026.
16 (*a*) A. S. Elgubbi, S. K. Ramadan, S. M. Gomha, M. E. A. Zaki and E. A. E. El-Helw, *Polycycl. Aromat. Compd.*, 2026, **46**(3), 283–302; (*b*) A. S. Elgubbi, E. A. E. El-Helw, M. S. Abousiksaka, A. Y. Alzahrani and S. K. Ramadan, *RSC Adv.*, 2024, **14**(26), 18417–18430.
17 S. Kamal, H. A. Derbala, S. S. Alterary, A. B. Bacha, M. Alonazi, M. K. El-Ashrey and N. N. El-Sayed, *ACS Omega*, 2021, **6**, 28992–29008.
18 C. K. Khatri, K. S. Indalkar, C. R. Patil, S. N. Goyal and G. U. Chaturbhuj, *Bioorg. Med. Chem. Lett.*, 2017, **27**, 1721–1726.
19 N. A. Osman, A. Ligresti, C. D. Klein, *et al.*, *Eur. J. Med. Chem.*, 2016, **122**, 619–634.
20 Q. Han, Z. Yin, J. Sui, Q. Wang and Y. Sun, *J. Braz. Chem. Soc.*, 2019, **30**, 1483–1497.
21 M. F. Mohamed, Y. M. Attia, S. A. Shouman and I. A. Abdelhamid, *Anti-Cancer Agents Med. Chem.*, 2017, **17**, 1084–1092.
22 R. Elrayess, Y. M. Abdel Aziz, M. S. Elgawish, M. Elewa, A. S. Yassen, S. S. Elhady, H. A. Elshihawy and M. M. Said, *Pharmaceuticals*, 2021, **14**, 9.
23 F. M. Sroor, M. M. Aboelenin, K. F. Mahrous, K. Mahmoud and A. H. M. Elwahy, *Arch. Pharm.*, 2020, **353**, 2000069.
24 T. Weinert, N. Olieric, R. Cheng, *et al.*, *Nat. Commun.*, 2017, **8**, 542.
25 W. Li, Y. Yin, W. Shuai, F. Xu, H. Yao, J. Liu, K. Cheng, J. Xu, Z. Zhu and S. Xu, *Bioorg. Chem.*, 2019, **83**, 380–390.
26 E. Z. Elrazaz, R. A. Serya, N. S. Ismail, D. A. Abou El Ella and K. A. Abouzid, Thieno[2,3-d]pyrimidine based derivatives as kinase inhibitors and anticancer agents, *Future J. Pharmaceut. Sci.*, 2015, **1**(2), 33–41.
27 E. A. E. El-Helw, A. Y. Alzahrani and S. K. Ramadan, Synthesis and antimicrobial activity of thiophene-based heterocycles derived from thiophene-2-carbohydrazide, *Future Med. Chem.*, 2024, **16**(5), 439–451.
28 Y. M. Youssef, M. E. Azab, G. A. Elsayed, A. A. El-Sayed, A. I. Hassaballah and E. A. E. El-Helw, *J. Iran. Chem. Soc.*, 2023, **20**(9), 2203–2216.
29 E. A. E. El-Helw, E. M. Hosni, M. Kamal, A. I. Hashem and S. K. Ramadan, Synthesis, insecticidal Activity, and molecular docking analysis of some benzo[h]quinoline derivatives against Culex pipiens L. Larvae, *Bioorg. Chem.*, 2024, **150**, 107591.

30 E. A. E. El-Helw, M. Asran, M. E. Azab, M. H. Helal and S. K. Ramadan, Synthesis, Cytotoxic, and Antioxidant Activity of Some Benzoquinoline-Based Heterocycles, *Polycycl. Aromat. Compd.*, 2024, **44**(9), 5938–5950.
31 E. A. E. El-Helw, M. Asran, M. E. Azab, M. H. Helal, A. Y. Alzahrani and S. K. Ramadan, Synthesis and in silico studies of certain benzo[f]quinoline-based heterocycles as antitumor agents, *Sci. Rep.*, 2024, **14**, 15522.
32 S. K. Ramadan, W. S. I. Abou-Elmagd, E. M. Hosni, M. Kamal, A. I. Hashem and E. A. E. El-Helw, Synthesis, in vivo evaluation, and in silico molecular docking of benzo [h]quinoline derivatives as potential Culex pipiens L. larvicides, *Bioorg. Chem.*, 2025, **154**, 108090.
33 M. M. Kaddah, A. A. Fahmi, M. M. Kamel, S. A. Rizk and S. K. Ramadan, Rodenticidal Activity of Some Quinoline-Based Heterocycles Derived from Hydrazide–Hydrazone Derivative. Polycyclic Aromat, *Compds*, 2023, **43**(5), 4231–4241.
34 E. A. E. El-Helw, W. S. I. Abou-Elmagd, E. M. Hosni, M. Kamal, A. I. Hashem and S. K. Ramadan, Synthesis of Benzo[h]quinoline Derivatives and Evaluation of Their Insecticidal Activity Against Culex pipiens L. Larvae, *Eur. J. Med. Chem.*, 2025, **290**, 117565.
35 C. H. Tseng, *et al.*, *Bioorg. Med. Chem.*, 2015, **23**, 141.
36 R. M. Humphries, J. Ambler, S. L. Mitchell, M. Castanheira, T. Dingle, J. A. Hindler, L. Koeth and K. Sei, CLSI methods development and standardization working group best practices for evaluation of antimicrobial susceptibility tests, *J. Clin. Microbiol.*, 2018, **56**(4), e01934.
37 B. Yang, Z. Lei, Y. Zhao, S. Ahmed, C. Wang, S. Zhang, S. Fu, J. Cao and Y. Qiu, Combination susceptibility testing of common antimicrobials in vitro and the effects of Sub-MIC of antimicrobials on Staphylococcus aureus biofilm formation, *Front. Microbiol.*, 2017, **8**, 1–14.
38 A. Baer and K. Kehn-Hall, Viral concentration determination through plaque assays: using traditional and novel overlay systems, *J. Visualized Exp.*, 2014, **93**, e52065.
39 S. K. Ramadan, H. S. Abd-Rabboh, A. A. Hafez and W. S. I. Abou-Elmagd, Some pyrimidohexahydroquinoline candidates: synthesis, DFT, cytotoxic activity evaluation, molecular docking, and in silico studies, *RSC Adv.*, 2024, **14**(23), 16584–16599.
40 https://www.rcsb.org/structure/9JNP.
41 https://www.rcsb.org/structure/5TW8.
42 https://www.rcsb.org/structure/4LXJ.
43 https://www.rcsb.org/structure/5NM5.
44 https://www.rcsb.org/structure/5CX6.
45 https://www.rcsb.org/structure/3PY7.
46 S. K. Ramadan, S. M. Gomha and E. A. E. El-Helw, Straightforward synthesis and in silico evaluation of pyrazolylthiazolidinone derivatives as prospective antiproliferative agents, *Bioorg. Chem.*, 2025, **165**, 109036.
47 A. H. Abdelrahman, M. E. Azab, M. A. Hegazy, A. Labena, A. Y. Alzahrani and S. K. Ramadan, Synthesis, Computational Analysis, and Exploring Antiproliferative Activity of Triazolo-and Thiazolo-Pyrimidine Derivatives as Potential EGFR Inhibitors, *J. Mol. Struct.*, 2025, **1333**, 141789.
48 A. El-Sewedy, A. R. Morsy, E. A. El-Bordany, N. F. Mahmoud, S. Z. Mohamed and S. K. Ramadan, Antiviral activity of newly synthesized pyrazole derivatives against Newcastle disease virus, *Sci. Rep.*, 2025, **15**, 18745.
49 A. Daina, O. Michielin and V. Zoete, *Sci. Rep.*, 2017, **7**, 42717.
50 E. A. E. El-Helw, S. K. Ramadan, S. M. Gomha and A. T. Ali, Synthesis and In Silico Evaluation of Thiazole, Thiazolidinone, and Pyrimidinethione Candidates Bearing A Benzo[h]quinoline Scaffold as Potential Antiproliferative Agents, *Polycycl. Aromat. Compd.*, 2026, **46**(2), 183–201.
51 A. K. El-Ziaty, W. S. I. Abou-Elmagd, S. K. Ramadan and A. I. Hashem, Synthesis and biological screening of some chromonyl-substituted heterocycles derived from 2(3H)-furanone derivative, *Synth. Commun.*, 2017, **47**(5), 471–480.
52 S. K. Ramadan and E. A. E. El-Helw, Synthesis and antimicrobial activity evaluation of some novel heterocycles derived from chromonyl-2(3H)-furanone, *J. Chem. Res.*, 2018, **42**(6), 332–336.
53 R. L. White, D. S. Burgess, M. Manduru and J. A. Bosso, Comparison of three different in vitro methods of detecting synergy: time-kill, checkerboard, and E test, *Antimicrob. Agents Chemother.*, 1996, **40**(8), 1914–1918.
54 A. Bahuguna, I. Khan, V. K. Bajpai and S. C. Kang, MTT assay to evaluate the cytotoxic potential of a drug, *Bangladesh J. Pharmacol.*, 2017, **12**(2), 115–118.
55 G. A. Costa, F. C. Rossatto, A. W. Medeiros, A. P. F. Correa, A. Brandelli, A. P. G. Frazzon and A. Motta, Evaluation antibacterial and antibiofilm activity of the antimicrobial peptide P34 against Staphylococcus aureus and Enterococcus faecalis, *An. Acad. Bras. Cienc.*, 2018, **90**(01), 73–84.